Title

Contribution of isoprene to chemical budgets: A model tracer study with the NCAR CTM MOZART-4

Journal

Journal of Geophysical Research, 113(D5)

ISSN

0148-0227

Authors

Pfister, GG
Emmons, LK
Hess, PG
et al.

Publication Date

2008-03-16

DOI

10.1029/2007jd008948

Contribution of isoprene to chemical budgets: A model tracer study with the NCAR CTM MOZART-4

G. G. Pfister,[1] L. K. Emmons,[1] P. G. Hess,[1] J.-F. Lamarque,[1] J. J. Orlando,[1] S. Walters,[1] A. Guenther,[1] P. I. Palmer,[2] and P. J. Lawrence[3]

Received 10 May 2007; revised 15 November 2007; accepted 12 December 2007; published 8 March 2008.

[1] We present a study of the sensitivity of isoprene emission calculations in a global chemistry transport model (CTM) to input land cover characteristics and analyze the impacts of changes in isoprene on the tropospheric budgets of atmospheric key species. The CTM Model for Ozone and Related Chemical Species, version 4 (MOZART-4) includes the online calculation of isoprene emissions based on the Model of Emissions of Gases and Aerosols from Nature (MEGAN), which is driven by three different land parameter inputs. We also included a tagging scheme in the CTM, which keeps track of the production of carbon containing species from isoprene oxidation. It is found that the amount of tropospheric carbon monoxide (CO), formaldehyde (HCHO) and peroxyacetylnitrate (PAN) explained by isoprene oxidation ranges from 9–16%, 15–27%, and 22–32%, depending on the isoprene emissions scenario. Changes in the global tropospheric burden with different land cover inputs can reach up to 10% for CO, 15% for HCHO, and 20% for PAN. Changes for ozone are small on a global scale, but regionally differences are as large as 3DU in the tropospheric column and as large as 5 ppbv in the surface concentrations. Our results demonstrate that a careful integration of isoprene emissions and chemistry in CTMs is very important for simulating the budgets of a number of atmospheric trace gases. We further demonstrate that the model tagging scheme has the capability of improving conventional methods of constraining isoprene emissions from space-borne HCHO column observations, especially in regions where a considerable part of the variability in the HCHO column is not related to isoprene.

Citation: Pfister, G. G., L. K. Emmons, P. G. Hess, J.-F. Lamarque, J. J. Orlando, S. Walters, A. Guenther, P. I. Palmer, and P. J. Lawrence (2008), Contribution of isoprene to chemical budgets: A model tracer study with the NCAR CTM MOZART-4, *J. Geophys. Res.*, *113*, D05308, doi:10.1029/2007JD008948.

1. Introduction

[2] Biogenic volatile organic compounds (BVOCs) play a significant role in determining the composition of the local, regional and global atmosphere. They react with hydroxyl radicals (OH), ozone (O_3) and nitrate radicals (NO_3) leading to the production of atmospheric key species such as carbon monoxide (CO) or formaldehyde (HCHO) [*Atkinson and Arey*, 1998]. BVOC oxidation is also a source of hydroperoxy and organic peroxy radicals, which can react with NO_x to stimulate O_3 production [*Cantrell et al.*, 1993], and of nitrogen-containing organics such as peroxy acetyl nitrate (PAN) which influence the global distribution of nitrogen oxides (NO_x) and thus indirectly impact O_3 production. Isoprene can also act as a sink for O_3 under low NO_x conditions [*Fan and Zhang*, 2004]. Former studies point out the important role of isoprene in atmospheric chemistry on a global scale [*Fehsenfeld et al.*, 1992; *Houweling et al.*, 1998; *Granier et al.*, 2000] as well as on regional scales [*Pierce et al.*, 1998; *Tao et al.*, 2003]. Recent studies have also confirmed significant secondary organic aerosol formation from BVOC emissions [*Hoffmann et al.*, 1998; *Griffin et al.*, 1999; *Henze and Seinfeld*, 2006]. Laboratory chamber studies of isoprene photooxidation show that SOA yields are 1–2% at high NO_x levels [*Kroll et al.*, 2005] and ~3% at low NO_x levels [*Kroll et al.*, 2006]. Through their effects on chemistry, aerosol concentrations and the global carbon cycle [*Fehsenfeld et al.*, 1992; *Lerdau et al.*, 1997], BVOC emissions exert a potentially significant influence on global climate [*Constable et al.*, 1999].

[3] Vegetation contributes about 90% of the non-methane VOCs emitted globally to the atmosphere, with isoprene providing the dominant contribution [*Guenther et al.*, 1995]. The factors controlling isoprene emissions include biological (such as type of vegetation or plant water stress) [*Guenther et al.*, 1993, 1995; *Harley et al.*, 1994; *Monson et al.*, 1994; *Pétron et al.*, 2001] physical (such as surface temperature and solar insolation) [*Guenther et al.*, 1995; *Sharkey et al.*, 2000] and chemical (such as ambient concentrations of O_3 and carbon dioxide) [*Rosenstiel et*

[1]National Center for Atmospheric Research, Boulder, Colorado, USA.
[2]School of GeoSciences, University of Edinburgh, Edinburgh, UK.
[3]Cooperative Institute for Research in Environmental Sciences (CIRES), University of Colorado, Boulder, Colorado, USA.

0148-0227/08/2007JD008948

al., 2003; *Velikova et al.*, 2005] variables. Chemical transport models generally include isoprene emission algorithms that parameterize these controlling factors.

[4] Estimates for global annual isoprene emissions found in the recent literature range from about 400–600 Tg C a^{-1}. *Guenther et al.* [1995] originally reported global annual emissions of ~500 Tg C a^{-1} but have recently refined this estimate to 440–660 Tg C a^{-1} [*Guenther et al.*, 2006]. *Shim et al.* [2005] estimate emissions as 375 Tg C a^{-1} in their CTM, but after constraining isoprene emissions with HCHO column observations from space they increase their value to 566 Tg C a^{-1}. Other modeling studies state values of 411 Tg C a^{-1} [*Folberth et al.*, 2005], 507 Tg C a^{-1} [*Levis et al.*, 2003], or 559 Tg C a^{-1} [*Potter et al.*, 2001].

[5] The biogenic emissions algorithm applied in the present study is MEGAN (Model of Emissions of Gases and Aerosols from Nature) developed by *Guenther et al.* [2006]. We have incorporated the MEGAN model in the chemical transport model MOZART (Model for OZone and Related chemical Tracers) and use this integrated system to study the role of isoprene on atmospheric composition with a focus on key species such as HCHO, CO, PAN or O_3. We also estimate current uncertainties in isoprene emission estimates related to land cover characteristics and investigate how these uncertainties translate into changes in the budgets of these trace gases. The sensitivity to the chemical oxidation scheme used is not a part of the present study.

[6] We incorporated a chemical tagging scheme into the MOZART model that keeps track of carbonaceous species produced from isoprene and that allows a precise determination of the trace gas budgets for contributions from isoprene. The chemical tagging scheme also has practical implications on the constraints of isoprene emissions from observations of atmospheric HCHO columns [*Chance et al.*, 2000; *Abbot et al.*, 2003]. To our knowledge this is the first comprehensive modeling analysis of the uncertainties in isoprene emissions related to land characteristics and how they impact the concentrations of a number of key atmospheric species on a global and regional scale. The purpose of the present study is to focus on the tagging scheme through model analysis and theoretical application; the evaluation with observations will be studied in future work.

[7] The outline of the paper is as follows. After discussing the model set-up and the simulations in sections 2 and 3, we describe the impacts of changes in isoprene emissions on atmospheric trace gas budgets (section 4). The nonlinearity in isoprene chemistry is discussed in section 4.4. In section 5 we present a synthetic mapping of isoprene emissions from HCHO column information using the chemical tagging scheme and we close with a summary in section 6.

2. Model Simulations

[8] The model simulations have been performed with the tropospheric chemistry transport model MOZART Version 4 [*Emmons et al.*, Sensitivity of chemical budgets to meteorology in MOZART-4, in preparation]. For the evaluation of the model we refer to *Emmons et al.* [*Sensitivity of chemical budgets to meteorology in MOZART-4,* in preparation], *Pfister et al.* [2005], and *Pfister et al.* [2006]. The spatial resolution of the model is set to 2.8 degrees by 2.8 degrees and the vertical resolution consists of 42 hybrid levels between the surface and 2 hPa. The model is driven by 6 hourly meteorological input fields from the NCEP-GFS (National Centers for Environmental Prediction Global Forecast System) analysis [http://www.nco.ncep.noaa.gov/pmb/products/gfs/; *Kanamitsu*, 1989]. Global fossil fuel and biofuel emissions for CO are taken from *Pétron et al.* [2004] and for other species from the European Union project POET (Precursors of Ozone and their Effects in the Troposphere) [*Granier et al.*, 2004]. Biomass burning emissions are based on GFED-v2 emissions [*van der Werf et al.*, 2006] scaled to Terra/MODIS (Moderate Resolution Imaging Spectroradiometer) fire counts for the specific time period. Emissions of isoprene are calculated online in the model as described in section 3. Methane concentrations in the model are specified at the lowest model boundary following observed methane distributions from the NOAA/ESRL Global Monitoring Division Global Cooperative Air Sampling Network [*Dlugokencky et al.*, 2005, 2007]. Model simulations were performed for a one year time period beginning in June 2005 with a spin-up phase of 1 year.

[9] Any representation of the complex non-methane hydrocarbon chemistry in the global model requires a rigorous selection of the most important reactions and species and a simplified NMHC chemistry. The chemical mechanism in MOZART-4 [*Emmons et al.*, in prep.; *Horowitz et al.*, 2007] contains a detailed treatment of hydrocarbon species containing three carbons or less, as well as a detailed representation of the chemistry of four lumped species that represent the larger alkanes, larger alkenes, monoterpenes and aromatics. For the most part, carbon is conserved in the model. However, as discussed in more detail below for isoprene, some complex and/or non-reactive species are not explicitly treated in the model, and thus are assumed to be lost exclusively to depositional processes.

[10] The treatment of isoprene is now further discussed. The gas phase chemistry of isoprene and its by-products is presented in Table 1 [see also *Horowitz et al.*, 2007]. Wet and dry deposition is included for stable intermediates, with rates taken from literature data or estimated by analogy to related species. Dry deposition velocities are determined online in the model, based on the resistance-based parameterization of *Wesely* [1989], *Walmsley and Wesely* [1996], and *Wesely and Hicks* [2000]. The deposition velocity calculation has been extended to take into account special cases for CO and H_2 [*Sanderson et al.*, 2003] and PAN [*Sparks et al.*, 2003]. Dry deposition rates for MACROOH, XOOH, and ISOPOOH are mapped to HNO_3 and HYAC and CH_3COOH to HCHO. The wet deposition calculation is based on the approach by *Giorgi and Chameides* [1985] using temperature dependent effective Henry's Law constants, with modifications as described by *Horowitz et al.* [2003]. Species mapping is done for ONIT, MACROOH, ISOPOOH (mapped to HNO_3), and for HYAC, HYDRALD, $ISOPNO_3$ (mapped to HCHO).

[11] Model runs showed, that, on a global scale, the oxidation of isoprene is initiated predominately by reaction with OH (~80%), with lesser contributions from O_3 (~15%) and NO_3 (~5%). Four sets of first-generation products from its OH-initiated oxidation are considered: (1) Methyl vinyl ketone (MVK) and methacrolein (MACR), and their co-product HCHO; (2) A lumped five-carbon

Table 1. MOZART-4 Photolysis and Gas Phase Chemistry Involving Isoprene and its Decomposition Product[a]

	A-Factor	-E/A
Photolysis Reactions		
MPAN + hυ → MCO_3 + NO_2		
MACR + hυ → 0.67*HO_2 + 0.33*MCO_3 + 0.67*HCHO + 0.67*CH_3CO_3 + 0.33*OH + 0.67*CO		
MVK + hυ → 0.7 * C_3H_6 + 0.7 * CO + 0.3 * CH_3O_2 + 0.3 * CH_3CO_3		
CH_3COCHO + hυ → CH_3CO_3 + CO + HO_2		
XOOH + hυ → OH		
ONITR + hυ → HO_2 + CO + NO_2 + HCHO		
ISOPOOH + hυ → 0.402 * MVK + 0.288 * MACR + 0.69 * HCHO + HO_2		
HYAC + hυ → CH_3CO_3 + HO_2 + HCHO		
GLYALD + hυ → 2 * HO_2 + CO + HCHO		
Gas-phase Chemical Reactions		
ISOP + OH → $ISOPO_2$ e.g., *tag: ISOP + OH → $ISOPO_2A$ + OH + ISOP*	2.54e-11	410
ISOP + O_3 → 0.4 * MACR + 0.2 * MVK + 0.07 * C_3H_6 + 0.27 * OH + 0.06 * HO_2 + 0.6 * HCHO + 0.3 * CO + 0.1 * O_3 + 0.2 * MCO_3 + 0.2 * CH3COOH e.g., *tag: ISOP + O_3 -> 0.4 * MACRA + 0.2 * MVKA + 0.07 * C_3H_6A + 0.6 * HCHOA + 0.3 * COA + 0.2 * MCO_3A + 0.2 * CH_3COOHA + O_3 + ISOP*	1.05e-14	−2000
$ISOPO_2$ + NO → 0.08 * ONITR + 0.92 * NO_2 + HO_2 + 0.55 * HCHO + 0.23 * MACR + 0.32 * MVK + 0.37 * HYDRALD e.g., *tag: $ISOPO_2A$ + NO -> 0.08 * ONITRA + 0.55 * HCHOA* + 0.23 * MACRA + 0.32 * MVKA + 0.37 * HYDRALDA + NO	2.2e-12	180
$ISOPO_2$ + NO_3 → HO_2 + NO_2 + 0.6 * HCHO + 0.25 * MACR + 0.35 * MVK + 0.4 * HYDRALD	2.4e-12	
$ISOPO_2$ + HO_2 → ISOPOOH	8.e-13	700
ISOPOOH + OH → 0.5 * XO_2 + 0.5 * $ISOPO_2$	3.8e-12	200
$ISOPO_2$ + CH_3O_2 → 0.25 * CH_3OH + HO_2 + 1.2 * HCHO + 0.19 * MACR + 0.26 * MVK + 0.3 * HYDRALD e.g., *tag: $ISOPO_2A$ + CH_3O_2 → 0.45 * CH_2OA + 0.19 * MACRA + 0.26 * MVKA + 0.3 * HYDRALDA + CH_3O_2*	5.e-13	400
*$ISOPO_2$ + CH_3O_2A → 0.25 * CH_3OHA + 0.75 * CH_2OA + $ISOPO_2$*		
$ISOPO_2$ + CH_3CO_3 → CH_3O_2 + HO_2 + 0.6 * HCHO + CO_2 + 0.25 * MACR + 0.35 * MVK + 0.4 * HYDRALD	1.4e-11	
MVK + OH → $MACRO_2$	4.13e-12	452
MVK + O_3 → 0.8 * HCHO + 0.95 * CH_3COCHO + 0.08 * OH + 0.2 * O_3 + 0.06 * HO_2 + 0.05 * CO + 0.04 * CH_3CHO	7.52e-16	−1521
MACR + OH → 0.5 * $MACRO_2$ + 0.5 * H_2O + 0.5 * MCO_3	1.86e-11	175
MACR + O_3 → 0.8 * CH_3COCHO + 0.275 * HO_2 + 0.2 * CO + 0.2 * O_3 + 0.7 * HCHO+ 0.215 * OH	4.4e-15	−2500
$MACRO_2$ + NO → NO2 + 0.47 * HO_2 + 0.25 * HCHO + 0.25 * CH_3COCHO + 0.53 * CH_3CO_3 + 0.53 * GLYALD + 0.22 * HYAC + 0.22 * CO	2.7e-12	360
$MACRO_2$ + NO → 0.8*ONITR	1.3e-13	360
$MACRO_2$ + NO_3 → NO_2 + 0.47*HO_2 + 0.25*HCHO + 0.25*CH_3COCHO + 0.22*CO + 0.53*GLYALD + 0.22*HYAC + 0.53*CH_3CO_3	2.4e-12	
$MACRO_2$ + HO_2 → MACROOH	8.e-13	700
$MACRO_2$ + CH_3O_2 → 0.73*HO_2 + 0.88*HCHO + 0.11*CO + 0.24*CH_3COCHO + 0.26*GLYALD + 0.26*CH_3CO_3 + 0.25*CH_3OH + 0.23*HYAC	5.e-13	400
$MACRO_2$ + $CH3CO_3$ → 0.25*CH_3COCHO + CH_3O_2 + 0.22*CO + 0.47*HO_2 + CO_2 + 0.53*GLYALD + 0.22*HYAC + 0.25*HCHO + 0.53*CH_3CO_3	1.4e-11	
MACROOH + OH → 0.5 * MCO_3 + 0.2*$MACRO_2$ + 0.1*OH + 0.2*HO_2	2.3e-11	200
MCO_3 + NO → NO_2 + HCHO + CH_3CO_3 + CO_2	5.3e-12	360
MCO_3 + NO_3 → NO_2 + HCHO + CH_3CO_3 + CO_2	5.e-12	
MCO_3 + HO_2 → 0.25*O_3 + 0.25*CH_3COOH + 0.75*CH_3COOOH + 0.75*O_2	4.30e-13	1040
MCO_3 + CH_3O_2 → 2 * HCHO + HO_2 + CO_2 + CH_3CO_3	2.0e-12	500
MCO_3 + CH_3CO_3 → 2 * CO_2 + CH_3O_2 + HCHO + CH_3CO_3	4.6e-12	530
MCO_3 + MCO_3 → 2 * CO_2 + 2 * HCHO + 2 * CH_3CO_3	2.3e-12	530
MCO_3 + NO_2 + M → MPAN + M		
MPAN + M → MCO_3 + NO_2 + M		
ISOP + NO_3 → $ISOPNO_3$ e.g., *tag: ISOP + NO_3 → $ISOPNO_3A$ + NO_3*	3.03e-12	−446
$ISOPNO_3$ + NO → 1.206 * NO_2 + 0.794 * HO_2 + 0.072 * HCHO + 0.167 * MACR + 0.039 * MVK + 0.794 * ONITR	2.7e-12	360
$ISOPNO_3$ + NO_3 → 1.206 * NO_2 + 0.072 * HCHO + 0.167 * MACR + 0.039 * MVK + 0.794 * ONITR + 0.794 * HO_2	2.4e-12	
$ISOPNO_3$ + HO_2 → 0.206 * NO_2 + 0.794 * HO_2 + 0.008 * HCHO + 0.167 * MACR + 0.039 * MVK + 0.794 * ONITR	8.e-13	700
CH_3COCHO + OH → CH_3CO_3 + CO + H_2O	8.4e-13	830
CH_3COCHO + NO_3 → HNO_3 + CO + CH_3CO_3	1.4e-12	−1860
ONITR + OH → HYDRALD + 0.4*NO_2 + HO_2	4.5e-11	
ONITR + NO_3 → HYDRALD + NO_2 + HO_2	1.4e-12	−1860
HYDRALD + OH → XO_2	1.86e-11	175
XO_2 + NO → NO_2 + 1.5*HO_2 + CO + 0.25*HYAC + 0.25*CH_3COCHO + 0.25*GLYALD	2.7e-12	360

Table 1. (continued)

Photolysis Reactions		
$XO_2 + NO_3 \rightarrow NO_2 + 1.5*HO_2 + CO + 0.25*HYAC + 0.25*CH_3COCHO + 0.25*GLYALD$	2.4e-12	
$XO_2 + HO_2 \rightarrow XOOH$	8.e-13	700
$XO_2 + CH_3O_2 \rightarrow 0.3 * CH_3OH + HO_2 + 0.7 * HCHO + 0.4 * CO + 0.1 * HYAC + 0.1 * CH_3COCHO + 0.1 * GLYALD$	5.e-13	400
$XO_2 + CH_3CO_3 \rightarrow CO + CH_3O_2 + 1.5 * HO_2 + CO_2 + 0.25 * HYAC + 0.25 * CH_3COCHO + 0.25 * GLYALD$	1.3e-12	640
$XOOH + OH \rightarrow H_2O + XO_2$	1.90e-12	190
$XOOH + OH \rightarrow H_2O + OH$		
$MPAN + OH \rightarrow 0.5*HYAC + 0.5*NO_3 + 0.5*HCHO + 0.5*HO_2 + 0.5*CO_2$ $k_o = 8.0e\text{-}27(T/300)^{-3.5}$; $k_\infty = 3.e\text{-}11$; $F_c = 0.5$		
$PAN + OH \rightarrow HCHO + NO_3 + CO_2$	4.e-14	
$HYAC + OH \rightarrow CH_3COCHO + HO_2$	3.e-12	
$GLYALD + OH \rightarrow HO_2 + 0.2*GLYOXAL + 0.8*HCHO + 0.8*CO_2$	1.e-11	

[a]For initial isoprene reactions we also give the tagged reactions as an example (tagged species indicated by suffix "A").

Species definitions:
ISOP: *isoprene* (C_5H_8)
ISOPO₂: *peroxy radical derived from OH + isoprene* ($HOCH_2COOCH_3CHCH_2$)
MACR: *methacrolein* (CH_2CCH_3CHO)
MVK: *methyl vinyl ketone* ($CH_2CHCOCH_3$)
MCO₃:*peroxy radical derived from abstraction reaction of OH with MACR* ($CH_2CCH_3CO_3$)
ONITR: *lumped isoprene nitrate* ($CH_2CCH_3CHONO_2CH_2OH$)
HYDRALD: *lumped unsaturated hydroxycarbonyl* ($HOCH_2CCH_3CHCHO$)
ISOPOOH: *unsaturated hydroxyhydroperoxide* ($HOCH_2COOHCH_3CHCH_2$)
HYAC: *hydroxyacetone* (CH_3COCH_2OH)
MACRO2: *peroxy radical from OH addition to MVK/MACR* ($CH_3COCHO_2CH_2OH$)
GLYALD: *glycolaldehyde* ($HOCH_2CHO$)
MPAN: *methacryloyl peroxynitrate* ($CH_2CCH_3CO_3NO_2$)
ISOPNO3: *peroxy radical from NO3 + isoprene* ($CH_2CHCCH_3OOCH_2ONO_2$)
XO2: *peroxy radical from OH+HYDRALD* ($HOCH_2COOCH_3CHCHOH$)

unsaturated hydroxycarbonyl species, e.g., $HOCH_2C(CH_3)=CHCHO$; (3) A lumped unsaturated hydroxy-hydroperoxide species, e.g., $HOCH_2CH(OOH)C(CH_3) = CH_2$; and (4) A lumped unsaturated hydroxynitrate species, e.g., $HOCH_2CH(ONO_2)C(CH_3) = CH_2$. A similar level of detail is used to describe the O_3-initiated isoprene chemistry, while the NO_3-initiated process is more heavily parameterized.

[12] The gas phase chemistry of MVK and MACR and its major by-products (methylglyoxal, hydroxyacetone, and glycolaldehyde) is reasonably well established, and is treated in detail in the model. On the other hand, the yields and ultimate atmospheric fate of the unsaturated hydroxycarbonyl, hydroxy-hydroperoxide and hydroxynitrate species have not been conclusively determined. Thus the OH-initiated degradation of these species is followed in the model using rate parameters and mechanisms estimated on the basis of established alkene oxidation pathways [e.g., *Atkinson*, 1997; *Orlando et al.*, 2003]. Most secondary products are followed through to completion in the gas phase, although some tri-functional species [e.g., $CH_3C(O)CH(OH)CH_2OH$] and/or non-reactive species are not included and thus are assumed to be lost exclusively via wet/dry deposition. It is estimated that ~80% of the isoprene carbon is followed to completion in the model (i.e., is either oxidized in the gas-phase to final end-products, CO and CO_2, or is lost explicitly via depositional processes). The remaining ~20% of the carbon is lost to the implicit deposition of the multifunctional and/or non-reactive species.

[13] The uncertainties with respect to yields of the species treated in detail in this study (CO, HCHO, and PAN) are difficult to estimate, given the unknowns alluded to above. However, an indication of possible uncertainties can be obtained from the sensitivity studies of *von Kuhlmann et al.* [2004]. These authors noted ±35% changes in global tropospheric CO and PAN production from isoprene in sensitivity studies carried out using different chemical mechanisms, different rate parameters and different assumptions regarding the deposition of intermediates. Larger changes are, of course, seen on regional scales. An additional low bias in our results (likely <10–15%) is present due to the implicit deposition of multifunctional/non-reactive isoprene by-products discussed above.

[14] Last, we note that the hydroxynitrate species (and related species generated from the NO_3-isoprene reaction) have drawn particular recent attention [*Liang et al.*, 1998; *Horowitz et al.*, 1998, 2007; *von Kuhlmann et al.*, 2004; *Fiore et al.*, 2005; *Wu et al.*, 2007; *Ito et al.*, 2007], as these compounds could have significant impacts on NO_x, and hence O_3 levels on regional to global scales. Of particular importance is whether the loss processes for these species act to re-release NO_x into the atmosphere, or to permanently remove it. The yield of hydroxy nitrates from reaction of OH/isoprene-derived peroxy radicals is assumed in the model to be 8%, in the middle of the range of available laboratory data (4–15%) [*Tuazon and Atkinson*, 1996; *Chen et al.*, 1998; *Chuong and Stevens*, 2002; *Sprengnether et al.*, 2002; *Patchen et al.*, 2007]. Again, we use the *von Kuhlmann et al.* [2004] study to provide an estimate of the global and regional effects of the uncertainties in the yield of the isoprene nitrates and their subsequent fate. When considering the global scale, effects do not appear to be large; only about a 10% change in the global contribution of isoprene to the PAN and CO burden is noted [*von Kuhlmann et al.*, 2004] when varying the isoprene nitrate

Table 2. Annual Average Isoprene Emissions (Tg C a^{-1}) for Various Regions Calculated in MOZART/MEGAN Using Different Sets of LAI and PFT Input[a]

	MODIS-L	MODIS-T	CLM
Global	470	600 (*28%*)	310 (*−34%*)
S-Hemisphere	271	326 (*20%*)	190 (*−30%*)
N-Hemisphere	202	276 (*37%*)	121 (*−40%*)
Australia	70	117 (*67%*)	49 (*−30%*)
Africa	106	130 (*23%*)	61 (*−42%*)
US cont.	23	31 (*35%*)	17 (*−26%*)

[a]Number in parentheses gives the percentage difference with respect to *MODIS-L*.

yield by a factor of two or changing the level of NO_x recycling that is occurring. As expected, however, effects on regional scales are more pronounced. As an example, the *von Kuhlmann et al.* [2004] study indicates that ozone decreases may be as large as 20% in some regions upon doubling the isoprene nitrate yield, and that PAN variations may be even larger (about ±50%).

3. Online Calculation of Isoprene Emissions in MOZART

[15] We included a simplified version of the Model of Emissions of Gases and Aerosols from Nature (MEGAN) [*Guenther et al.*, 2006] into MOZART for online calculation of the emissions of isoprene into the atmosphere. MEGAN estimates the net emission rate of isoprene (and other biogenic VOCs) as

$$\text{Emission} = [\varepsilon][\gamma][\rho]$$

where $[\varepsilon]$ is the emission factor for a specific vegetation category, $[\gamma]$ an emission activity factor accounting for environmental conditions (e.g., leaf area index, solar radiation and temperature, etc.), and $[\rho]$ a factor accounting for loss and production within the canopy. The version currently included in the CTM does not include a biogenic emission dependence on soil moisture and past weather and uses a parameterized canopy environment model. These simplifications are significant for daily variability and local scales but have minor impact when averages over larger regions (e.g., continents) or longer times (e.g., a month) are considered or when differences between different land parameters are examined.

[16] Driving variables for MEGAN include current temperature and solar radiation, and land cover data including leaf area index (LAI), plant functional type (PFT), and landcover species composition. Regional differences in predicted isoprene emissions can be up to a factor of 3 for specific times and locations in MEGAN depending on the driving variables with LAI and PFT being two of the dominant factors [*Guenther et al.*, 2006]. Here we focus on sensitivities of MEGAN to land cover information only and do not consider uncertainties in other driving variables or as caused by parameterizations.

[17] We run MOZART/MEGAN with three different sets of satellite derived LAI and PFT input data, all of which have been developed for inclusion in the Community Land Model (CLM) [*Bonan et al.*, 2002a] and refer to the 17 vegetation classes defined in the CLM. The original land surface parameters of the CLM are based on AVHRR (Advanced Very High Resolution Radioameter) data [*Bonan et al.*, 2002b]. Recent satellite imagery from the Moderate Resolution Imaging Spectroradiometer (MODIS) provides global land surface data with hitherto unavailable spatial, temporal, and spectral resolution [*Justice et al.*, 2002] and recent studies have identified significant differences between the current land surface parameters of the CLM and land surface mapping products from MODIS [*Oleson et al.*, 2003; *Tian et al.*, 2004; *Lawrence and Chase*, 2007]. We examine in this study differences between the original CLM PFT and LAI maps (in the following referred to as "CLM") and two MODIS-based LAI and PFT maps. One, defined here as "MODIS-L" is described in detail by *Lawrence and Chase* [2007], and the other ("MODIS-T") is described by *Tian et al.* [2004]. Even though both maps are based on the same satellite imagery, there can be quite significant differences in the derived PFT and LAI data due to the different approaches for mapping. A main distinction is that the mapping used by *Lawrence and Chase* [2007] captures multiple PFTs for one grid cell, while the approach by *Tian et al.* [2004] uses a single PFT.

[18] Compared to the original CLM data set the new parameters show substantially higher LAI with the largest increases in tropical forest. The new parameters also have an increase in bare soil fraction and broadleaf trees over all land surface, and a strong decrease in grassland area. A discussion of detailed regional and seasonal differences goes beyond the scope of this paper, and the reader is referred to the studies by *Tian et al.* [2004] and *Lawrence and Chase* [2007], where the mapping technique as well as changes in new parameters compared to the CLM vegetation maps are discussed in greater detail.

[19] The 17 PFT categories have been combined into five categories in MOZART: broadleaf trees, fine leaf trees, shrubs, grass and crops. MEGAN assigns geographically varying emission factors to each vegetation category. For example, each location in the MOZART domain is assigned an isoprene emission factor for broadleaf trees that is based on the broadleaf tree species composition at that location. The species-specific emission factors used in MEGAN are described by *Guenther et al.* [2006]. At the time of this study, geographically varying emission factors were available from MEGAN for the first three categories [*Guenther et al.*, 2006], and a single global value has been used for grass (0.3 mg isoprene m^{-2} h^{-1}) and crops (0.1 mg isoprene m^{-2} h^{-1}). From these five land cover types, broadleaf trees and shrubs feature the highest average isoprene emission factors with emission factors in the range of 0.1–30 mg isoprene m^{-2} h^{-1}.

[20] Large uncertainties in the isoprene emissions are found depending on the LAI and PFT input used. Table 2 lists total isoprene emissions for various regions calculated with the three sets of input parameters mentioned above. Generally, *MODIS-T* yields the highest emission strength and *CLM* the smallest. The global estimates are on the same order as the values found in the literature, with *MODIS-T* and *CLM* on the higher and lower end, respectively. Figure 1 displays maps of isoprene emissions calculated with *MODIS-L* LAI and PFT data. Regions with the largest isoprene sources are found where high biomass density,

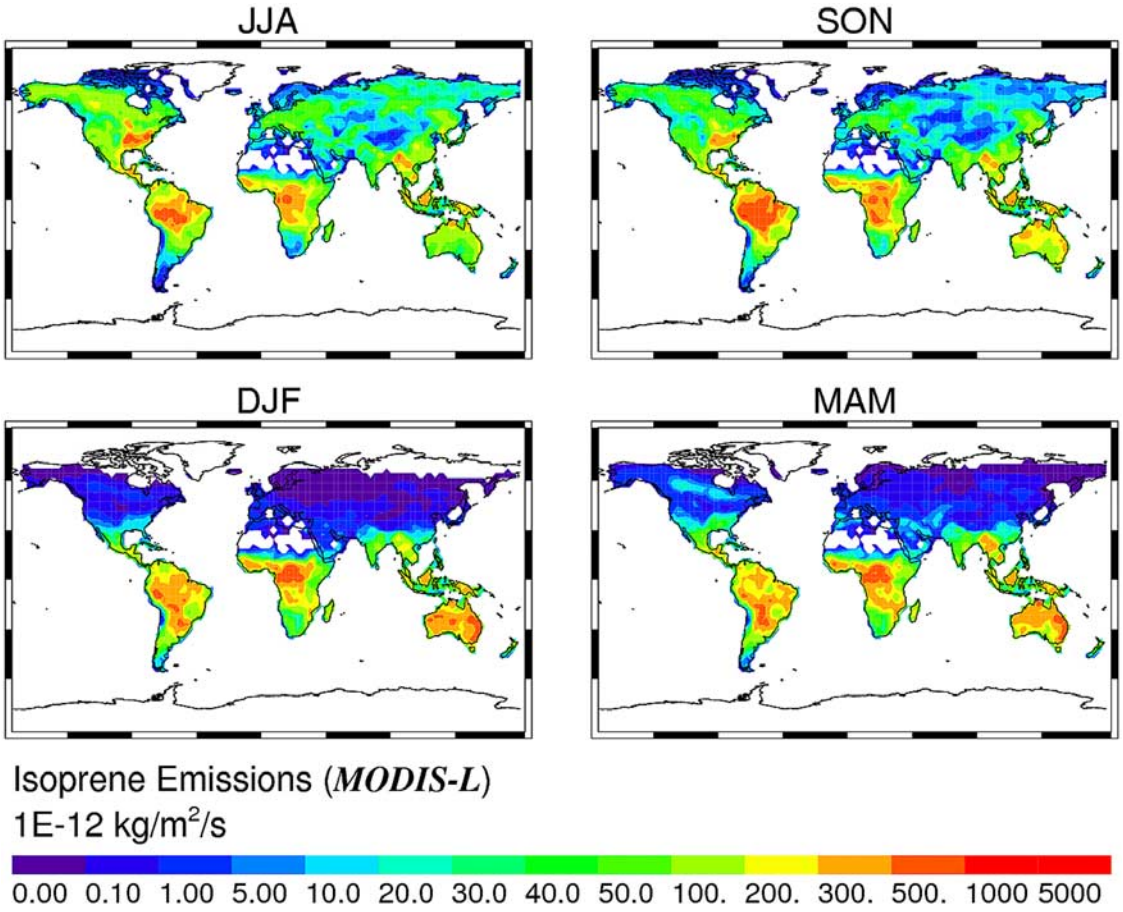

Figure 1. Isoprene emissions calculated in MOZART using *MODIS-L* input data for different seasons.

high temperatures and strong insolation occur. The Tropics stand out as a strong source region year-round and in the Southern Hemisphere the largest isoprene emitting regions are identified as North-Central South America, Equatorial Africa and Australia. In the Northern Hemisphere we see the largest isoprene emissions over the southeastern part of the US, which is explained by the prevalence of broadleaf trees in that region.

[21] All data sets predict lower emissions for the Northern Hemisphere compared to the Southern Hemisphere, where less area is covered by land but where source magnitudes are stronger. The South to North Hemispheric ratio is higher for *CLM* (1.6) than for *MODIS-L* (1.34) or *MODIS-T* (1.18). The source distribution between all three input sets features similar large-scale patterns. The spatial variability, however, can be quite large as seen from the maps in Figure 2 where we show differences in emissions calculated using *MODIS-T* and *CLM* relative to *MODIS-L*. Largest regional differences between the three data sets are seen over Australia, Africa, and the continental US (Table 2). In order to better understand these differences we performed offline calculations of isoprene emissions separated by vegetation class and only considering the dependence on PFT (emission = emission factor•PFT) and on PFT and LAI combined (emission = emission factor•PFT•γ_{LAI} with γ_{LAI} calculated according to equation 15 by *Guenther et al.* [2006]). No other driving variables are taken into account. These calculations show that, on a global scale, broadleaf trees and shrubs dominate isoprene emissions. If only PFT distributions are considered, broadleaf trees account for about 44% of global isoprene emissions in *CLM*, 52% in *MODIS-T* and 52% in *MODIS-L* (Table 3). Shrubs account for most of the remainder. The weight is shifted more strongly toward broadleaf trees when LAI values are added to the calculations. The generally lower values for *CLM* compared to the MODIS-based maps are explained by significantly smaller contributions from mostly broadleaf tree contributions as well as smaller LAI values (Table 3), while the larger global isoprene emissions in *MODIS-T* compared to *MODIS-L* are only explained when LAI dependencies are included. *MODIS-T* shows significantly higher contributions from shrubs compared to the other maps.

[22] In general, it is differences in the coverage of either broadleaf trees or shrubs between the land parameter maps that drive most of the regional differences in isoprene emissions, because these are the vegetation classes with the highest emission factors. The large values in *MODIS-T* over Australia are driven by the large coverage and high LAI values associated with shrubs (57% of the total isoprene emissions). The contribution from shrubs in *MODIS-T* is about a factor of 2.5 higher compared to *MODIS-L* and a factor of 4 higher compared to *CLM*. Over Africa it is mostly differences in broadleaf trees that account for the discrepancies between the vegetation maps (contributing 95% to the total isoprene emissions in *MODIS-L* and *CLM* and 85% in *MODIS-T*). Only *MODIS-T* shows appre-

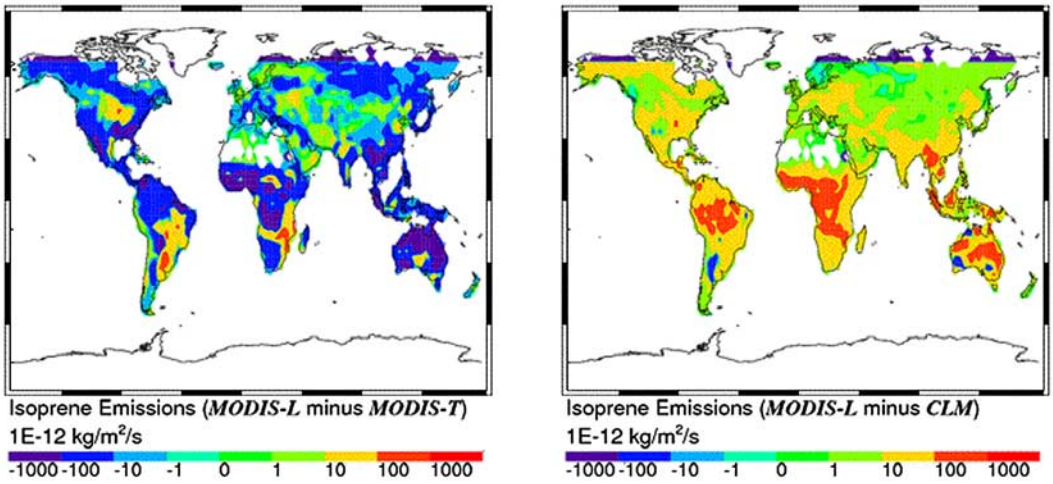

Figure 2. Annually averaged difference (absolute values) between isoprene emissions calculated in MOZART with *MODIS-T* and CLM compared to *MODIS-L*.

ciable amounts from shrubs (12% of the total isoprene emissions) over this region. The US is dominated by emissions from broadleaf trees (72–77% depending on the vegetation map used), needleleaf trees account for 7–11% and shrubs for about 10% in *CLM* and *MODIS-L*, but 20% in *MODIS-T*.

[23] The topic of the present study is to find out to what degree isoprene in general and differences in isoprene emission inventories affect tropospheric composition. We focus on chemical fields derived in different model simulations performed with MOZART-4. Three simulations include isoprene with the emissions calculated by either using *MODIS-L, MODIS-T,* or *CLM* as input. In a fourth model run the emissions of isoprene are set to zero ("*noISOP* simulation"). We consider the *MODIS-L* simulation as our standard case, and if not specified otherwise, the analysis refers to this scenario.

[24] To study the role of isoprene on determining global chemical oxidant budgets we also added a chemical tagging scheme to the model to track the production of CO and other carbon-containing isoprene oxidation products. In this scheme, each carbon compound derived from isoprene is treated as a separate species, allowing us to determine the amount of carbonaceous species such as CO or HCHO produced from isoprene oxidation. The tagging is set up to track the mass of the species and does not affect the original mechanism. To demonstrate this we include in Table 1 example reactions for the tagged species.

[25] The tagging scheme in combination with the *noISOP* model simulations also allows an investigation of the non-linear effects of isoprene oxidation on tropospheric chemistry. Quantifying the contribution of isoprene to tropospheric chemistry would not be possible by only turning off isoprene emissions because this would also change the oxidation capacity of the chemical system. In the simulation using *MODIS-L* we tagged, in addition to the isoprene pathway, the formation of carbon species from methane oxidation. Tagged species from isoprene are defined in the following notation as $SPECIES_{ISOPRENE}$ (e.g., $CO_{ISOPRENE}$) and from methane as $SPECIES_{METHANE}$ (e.g., $CO_{METHANE}$).

4. Impact of Isoprene on Global and Regional Trace Gas Budgets

4.1. Carbon Monoxide

[26] CO is a common product from the oxidation of hydrocarbons and plays a major role in tropospheric chemistry by controlling much of the OH abundance [*Warneck*, 2000]. The global annual source of CO in the model is calculated as 2544 Tg CO a^{-1}. Direct emissions contribute 1200 Tg CO a^{-1} and the photochemical production using *MODIS-L* contributes 1354 Tg CO a^{-1}. On a global annual

Table 3. Contribution (%) of Different Vegetation Classes to Total Isoprene Emissions for CLM, MODIS-T and MODIS-T When Considering Dependence on PFT (1) and on PFT and LAI Combined (2)[a]

	(1) Emissions = f(PFT)			(2) Emissions = f(PFT and LAI)		
	CLM	M-T	M-L	CLM	M-T	M-L
Needleleaf	5% (0.76)	6% (1.23)	5%	9% (0.78)	8% (1.28)	8%
Broadleaf	44% (0.70)	52% (0.94)	52%	71% (0.70)	68% (1.18)	76%
Shrubs	49% (0.98)	41% (0.93)	41%	11% (0.52)	23% (2.19)	14%
Grass	2% (1.22)	1% (0.50)	2%	2% (1.11)	1% (0.72)	1%
Crop	<1% (1.20)	<1% (0.84)	<1%	<1% (1.23)	<1% (0.99)	<1%
All	100% (0.83)	100% (0.94)	100%	100% (0.68)	100% (1.31)	100%

[a]Values in parenthesis specify the ratio of CLM and MODIS-T to MODIS-L.

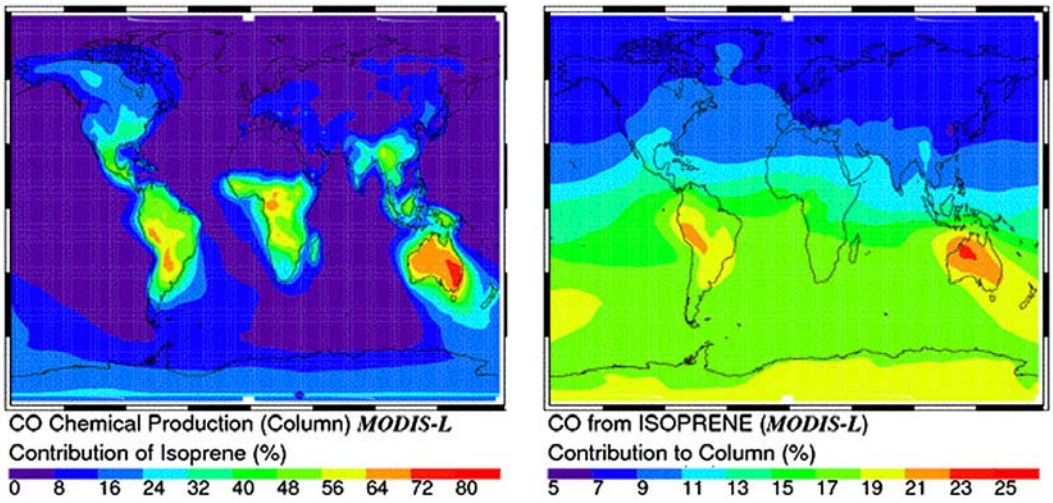

Figure 3. CO chemical production from isoprene oxidation (left) and contribution (%) of CO from isoprene oxidation to the total CO column. *MODIS-L* simulation, annual average.

average, the oxidation of methane (687 Tg CO a^{-1}) and isoprene (331 Tg CO a^{-1}) represent the first and second largest contributions to CO chemical production.

[27] The global yield for CO from isoprene on a per carbon basis as calculated by dividing the global $CO_{ISOPRENE}$ production by the global isoprene source is 0.30, in agreement with the study by *Miyoshi et al.* [1994] and slightly larger than the estimate of 0.23 by *Granier et al.* [2000]. *Duncan et al.* [2007] report a value of 0.20 and *Bergamaschi et al.* [2000] of 0.34. CO production from isoprene is typically more efficient in polluted (high NO_x) regions [*Miyoshi et al.*, 1994]. For example, a yield of 0.38 is derived for the continental US, and a yield of 0.25 is calculated over Australia or South America.

[28] Photochemical CO production on the global scale is largely driven by methane oxidation. With methane being distributed fairly uniformly in the atmosphere, the driving variable is OH and thus the amount of solar radiation. This results in a first-order meridional structure with highest values over the tropics and values decreasing toward the poles. The chemical production is larger over the Summer, compared to the Winter, Hemisphere. Methane oxidation is the dominant contributor to CO mostly over ocean regions where it accounts for 70–90% of the total photochemical production, but over continents its contribution might be as low as 10%. This is because of the increased importance of photochemical production of CO from isoprene (and other VOCs) over continents.

[29] The annually averaged photochemical production of CO from isoprene is illustrated in Figure 3. Because of the short lifetime of isoprene, the distribution of CO production from isoprene is largely dependent on the isoprene source distribution itself. CO production from isoprene oxidation has significant values over and downwind of high isoprene emitting regions, where it generally dominates over methane oxidation, but is rather insignificant outside these domains. For most of the high isoprene emitting regions such as Australia, South Equatorial Africa, South America or the summertime Eastern US isoprene oxidation contributes 50–80% of the total production of CO. During Southern Hemispheric wintertime there is a clear impact of isoprene on Antarctic chemistry when CO and CO precursors have a long enough lifetime to be transported over large distances.

[30] The global annual burden of CO in the troposphere (surface to 100 hPa) that results from direct and indirect CO sources can differ by 10% depending on the LAI and PFT data set used by the model. We derive a burden of 402 Tg CO for *MODIS-L*, 427 Tg CO for *MODIS-T*, and 376 Tg CO for *CLM* (Table 4). 13% of the total CO burden is due to isoprene (16% for *MODIS-T*, 9% for *CLM*), and 25% due to methane oxidation. These results are comparable to the study by *Granier et al.* [2000] who estimated the contribution of isoprene to the global CO burden as 10% and of methane as 27%. More than half (~60%) of the photochemical CO production from isoprene takes place below

Table 4. Total and Isoprene Related Burden for the Range Surface-100 hPa and the Range Surface-800 hPa for CO (Tg CO), HCHO (Tg HCHO) and PAN (Tg N)[a]

	Burden Surface-100 hPa						Burden Surface-800 hPa					
	Total			Isoprene			Total			Isoprene		
PFT/LAI	M-L	M-T	CLM	M-L	M-T	CLM	M-L	M-T	CLM	M-L	M-T	CLM
CO	402	427	376	54 *13%*	69 *16%*	35 *9%*	94	99	88	12 *12%*	15 *15%*	8 *9%*
HCHO	0.97	1.03	0.90	0.21 *22%*	0.28 *27%*	0.13 *15%*	0.42	0.45	0.38	0.13 *30%*	0.16 *36%*	0.08 22%
PAN	0.246	0.266	0.22	0.070 *29%*	0.085 *32%*	0.049 *22%*	0.037	0.040	0.035	0.007 *18%*	0.009 *21%*	0.005 13%

[a]The percentage value gives the relative contribution of the species created from isoprene to the total amount. Values are specified for simulations using either *MODIS-L* (abbreviated as M-L), *MODIS-T* (abbreviated as M-T) or *CLM* in the calculations of isoprene emissions.

Table 5. Atmospheric Lifetime of CO (Days) and HCHO (Hours) for the Different Isoprene Scenario Simulations for Five Latitudinal Bands and for the Entire Globe[a]

		MODIS-L	MODIS-T	CLM	noISOP
CO Lifetime (days)	*60N-90N*	269	282	254	257
	30N-60N	95	98	92	92
	Tropics	62	66	59	57
	60S-30S	139	146	138	138
	90S-60S	375	384	378	396
	Global	**83**	**87**	**80**	**78**
HCHO Lifetime (hours)	*60N-90N*	12.3	12.7	12.1	12.3
	30N-60N	8.3	8.5	8.2	8.2
	Tropics	7.8	8.0	7.5	7.0
	60S-30S	9.6	9.9	9.5	9.1
	90S-60S	14.3	14.9	14.1	13.7
	Global	**8.1**	**8.4**	**7.9**	**7.6**

[a]Lifetimes are derived by dividing the total burden of the particular region by the according loss rate.

800 mbar; however, as a result of the week-to-monthlong lifetime, CO can be transported over large distances and for this reason the fraction of CO from isoprene to the total burden depends very weakly on the altitude range considered. Changing isoprene emissions also impacts the lifetime of CO (Table 5) with changes on the order of a few days possible. In the tropics where the average lifetime of CO is about two months, we find differences between the three isoprene scenarios of up to 6 days.

[31] Figure 3 illustrates the annually averaged relative contribution of CO from isoprene oxidation to the total CO column. Direct emissions of CO are largest over the industrial areas of the Northern Hemisphere and during times of strong biomass burning [*Edwards et al.*, 2004, 2006]. For most of these regions, CO from direct emissions generally dominates over photochemically produced CO. The sources of isoprene, however, frequently collocate with regions of high direct emissions, in particular wildfires, and can account for up to one-third of the CO load. The portion of the total CO loading that can be explained by methane oxidation is typically below 15% in continental regions.

[32] The contributions of isoprene to the CO column range from a few percent during Northern Hemispheric wintertime up to 30%. The highest contributions are found near regions with large isoprene emissions such as parts of the Southern Hemisphere, with the "hot spot" being Australia, and to a lesser extent (~10–15%) the Eastern US during summer and fall. This implies that an uncertainty of, e.g., 50% in isoprene emissions can translate into an up to 15% uncertainty in the total CO column. The frequency distribution functions for differences in the CO column amount between the four model simulations are illustrated in Figure 4 using the *MODIS-L* simulation as the reference case. The CO column increases by up to 30% (or $7 \cdot 10^{17}$ cm^{-2}) upon inclusion of isoprene. Using different LAI and PFT sets results in uncertainties in the modeled CO column of the order of ±20% (or $\pm 5 \cdot 10^{17}$ cm^{-2}). Northern Australia and Equatorial Africa are among the regions with the largest uncertainties.

[33] Similar contributions and uncertainties are estimated for the CO surface mixing ratio (graphs not shown here). Over high isoprene emitting regions, isoprene contributes 30–40 ppbv to monthly mean surface CO levels. The relative fraction over the Eastern US in summertime is 15–20%, over Australia it can be as high as 30%. Because of transport of $CO_{ISOPRENE}$ and its precursors, high contributions are also evident in remote regions, e.g., 20–25 ppbv over parts of the South Pacific and Indian Ocean. Different isoprene emission scenarios can change the surface CO mixing ratio by about ±20% (±15 ppbv).

[34] In Figure 5 we summarize the results for the globe and selected regions by showing monthly mean total CO columns as well as the corresponding absolute and fractional contributions from methane and isoprene oxidation. Results are included for simulations with *MODIS-L*, *MODIS-T*, and *CLM*. The highest CO amounts are generally estimated with *MODIS-T* due to high isoprene emissions, and differences in the contributions reach 10–15% regionally between the different LAI and PFT inputs. A similar seasonality is seen in all of the different emission scenarios.

[35] On a global average we see the dominance of methane over isoprene with contributions of roughly one-quarter and one-eighth to the total CO, respectively. The annual variability is small. Results for remote oceanic regions are similar to the globe as a whole, which is explained by the long lifetime of CO allowing for transport away from source regions.

[36] The Eastern US and China have the highest CO amounts in springtime, which is due to the long lifetime of CO during wintertime and its accumulation in the atmosphere. Maximum $CO_{ISOPRENE}$ is seen in summertime when vegetation is most active and temperatures highest. This

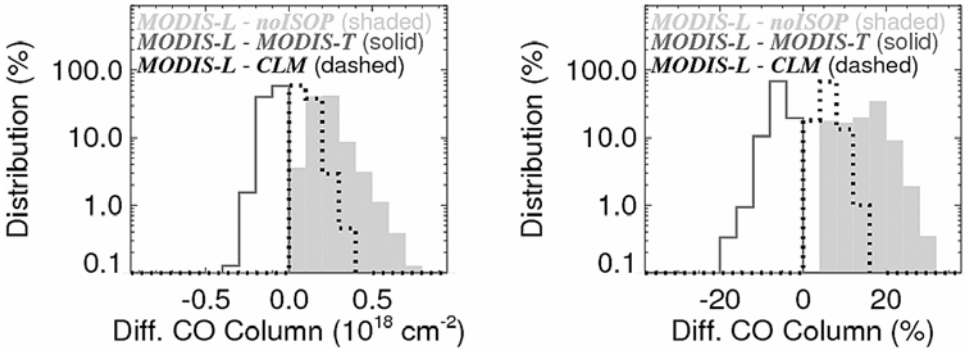

Figure 4. Absolute and relative difference in the CO column between *MODIS-L*, *MODIS-T*, *CLM* and *noISOP* simulations. Distribution functions are calculated from monthly mean CO fields.

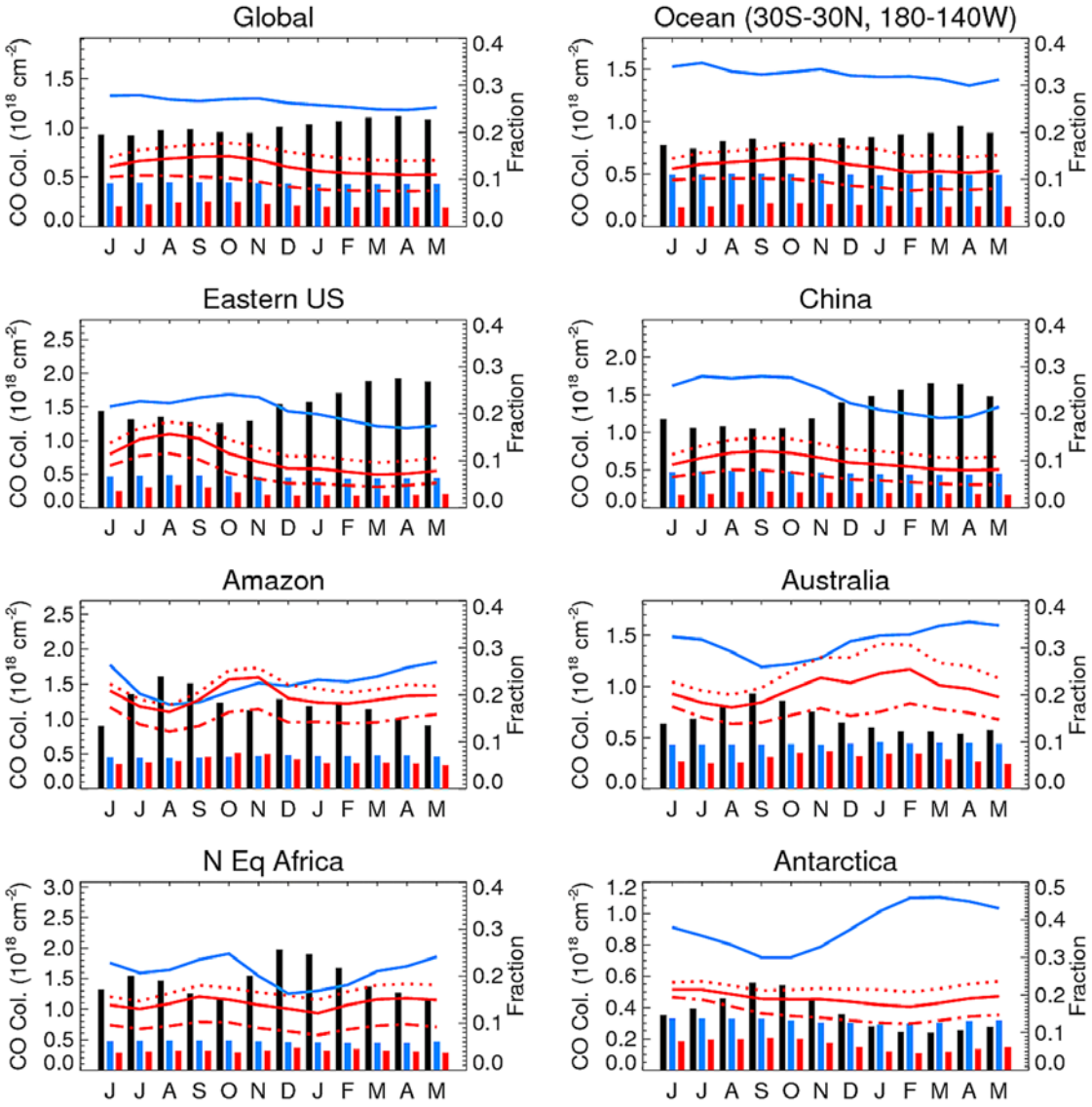

Figure 5. Monthly CO column and contributions from methane and isoprene oxidation for individual regions. Left ordinate: absolute column (*MODIS-L* simulation) due to isoprene (red bars), methane (blue bars), and others (black bars). Right ordinate: relative contributions to the total column from methane (blue line) and isoprene (red line). Solid lines denote results for *MODIS-L*, dashed lines for *MODIS-T*, dash-dotted lines for *CLM*.

coincides with the season when CO emissions from sources other than isoprene and methane are at their minimum, thus isoprene somewhat reduces the amplitude of the seasonal cycle in these regions. China shows a weaker seasonality in $CO_{ISOPRENE}$ due to its proximity to the equator.

[37] $CO_{ISOPRENE}$ for the Amazon region (North-Central South America) and for North Equatorial Africa has a less pronounced seasonality. Maxima in the CO columns over the Amazon from July to September are explained by biomass burning in this region, and around January by transport of biomass burning plumes from North Equatorial Africa. Hence the lowest relative contributions of $CO_{ISOPRENE}$ are estimated during the times of peak CO. Australia shows highest CO columns during the biomass burning season from August to October, and largest $CO_{ISOPRENE}$ during Southern Hemispheric summertime, thus isoprene slightly impacts the CO seasonal cycle. While all other regions have maximum contributions from direct local CO sources, CO over Antarctica is dominated by transport of CO and CO precursors. The maximum occurs during Southern Hemispheric winter, when the CO lifetime is long enough to allow transport from lower latitudes toward the pole. Over Australia and Antarctica, methane and isoprene oxidation account for more than half of the CO load in the atmosphere.

4.2. Formaldehyde

[38] Formaldehyde (HCHO) is a high yield oxidation product of VOCs and its total chemical production in the atmosphere is estimated as 1321 Tg HCHO a^{-1} (*MODIS-L*). In comparison, direct emissions of HCHO are of the order

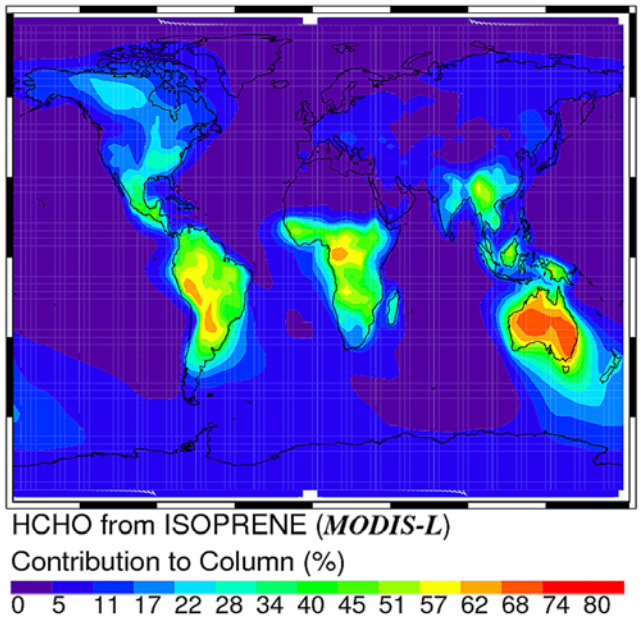

Figure 6. Annually averaged contribution (%) of isoprene oxidation to the total formaldehyde column (*MODIS-L*).

of 5 Tg HCHO a^{-1} and play only a minor role in the global budget. The atmospheric HCHO background is controlled by methane oxidation, and the global contribution from isoprene in the model is 18% (240 Tg HCHO a^{-1}) for emissions calculated with *MODIS-L,* and 22% for *MODIS-T* and 12% for *CLM*. The global annually averaged burden (surface to 100 hPa) of HCHO is 0.97 Tg HCHO with 22% explained by isoprene and 48% by methane oxidation, and the remainder mostly from the oxidation of anthropogenic VOCs. Simulations with *MODIS-T* yield a global burden of 1.03 Tg HCHO with 27% from isoprene oxidation while simulations with *CLM* result in 0.90 Tg HCHO and 15% from isoprene (Table 4). The contributions are larger when considerations are limited to the burden of the lower troposphere (22–36%). A large part of the HCHO is produced at low altitudes and as a result of its short lifetime (Table 5) it is not very efficiently transported to the higher atmosphere. The yield for HCHO from isoprene on a per carbon basis is estimated as 0.22 averaged over the globe for a year. As for CO, the yield is typically higher in high NO_x regimes compared to low NO_x regimes. Annual averaged yields over the Eastern US are on the order of 0.27 and over Australia on the order of 0.20.

[39] The contribution of isoprene oxidation to HCHO columns (Figure 6) has a high spatial variability that results from the fairly short formaldehyde lifetime (on the order of hours during summertime). In comparison, the contribution of isoprene to the longer lived species CO (Figure 3) showed larger scale patterns. Over high isoprene emitting regions more than half of the total column amount of HCHO may be due to isoprene oxidation, while further away from these source regions, the contributions can drop to nearly zero. Australia again stands out, showing the highest contributions of up to 80% for *MODIS-L*. *MODIS-T* and *CLM* show similar spatial distributions, with contributions of a few percent higher and lower, respectively.

[40] Because of the strong impact of isoprene on HCHO formation and its short lifetime, HCHO amounts are highly sensitive to the location and magnitude of isoprene emissions. Figure 7 shows the distribution function of differences in the HCHO column for the individual isoprene emission scenarios. Including isoprene can increase the HCHO column by up to 70% ($\sim 1 \cdot 10^{16}$ cm^{-2}) and different LAI and PFT data sets cause uncertainties of up to ±50% ($5 \cdot 10^{15}$ cm^{-2}). The largest discrepancy in the HCHO columns when applying different LAI and PFT input are found, as for CO, over Australia and equatorial Africa.

[41] The monthly mean total HCHO columns for individual regions and absolute and relative contributions from $HCHO_{ISOPRENE}$ and $HCHO_{METHANE}$ are summarized in Figure 8. The relative importance of isoprene compared to methane oxidation changes between regions and can also change between seasons. Over remote oceanic regions the impact of isoprene is negligible because of the short lifetime of isoprene and HCHO. For the Eastern US, HCHO columns during summertime are controlled by isoprene (which accounts for about half of the total HCHO column), but are controlled by methane outside the growing season. For Amazon and Australia, isoprene is dominant throughout the year. Little difference in $HCHO_{ISOPRENE}$ contributions between *MODIS-L* and *MODIS-T* simulations is found for the Amazon, while absolute differences can be as high as 15% over Australia. *CLM* simulations are generally lower by up to 20–25% compared to the other data sets and in some cases also exhibit differences in the seasonality (e.g., Australia or North Equatorial Africa).

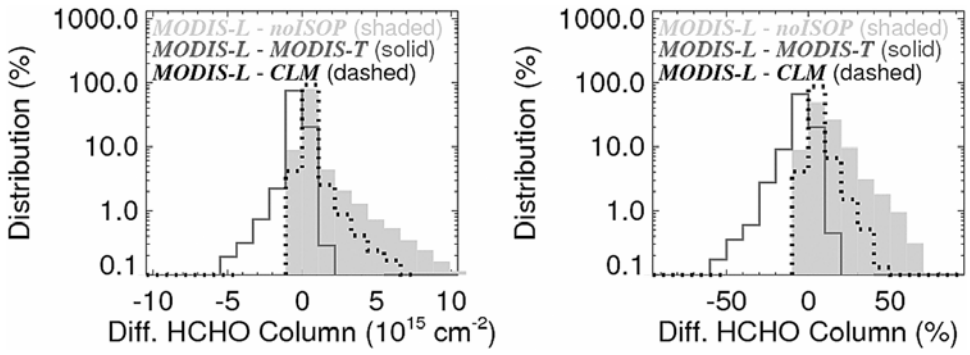

Figure 7. Absolute and relative difference in the HCHO column between *MODIS-L*, *MODIS-T*, *CLM,* and *noISOP* simulations. Distribution functions are calculated from monthly mean HCHO fields.

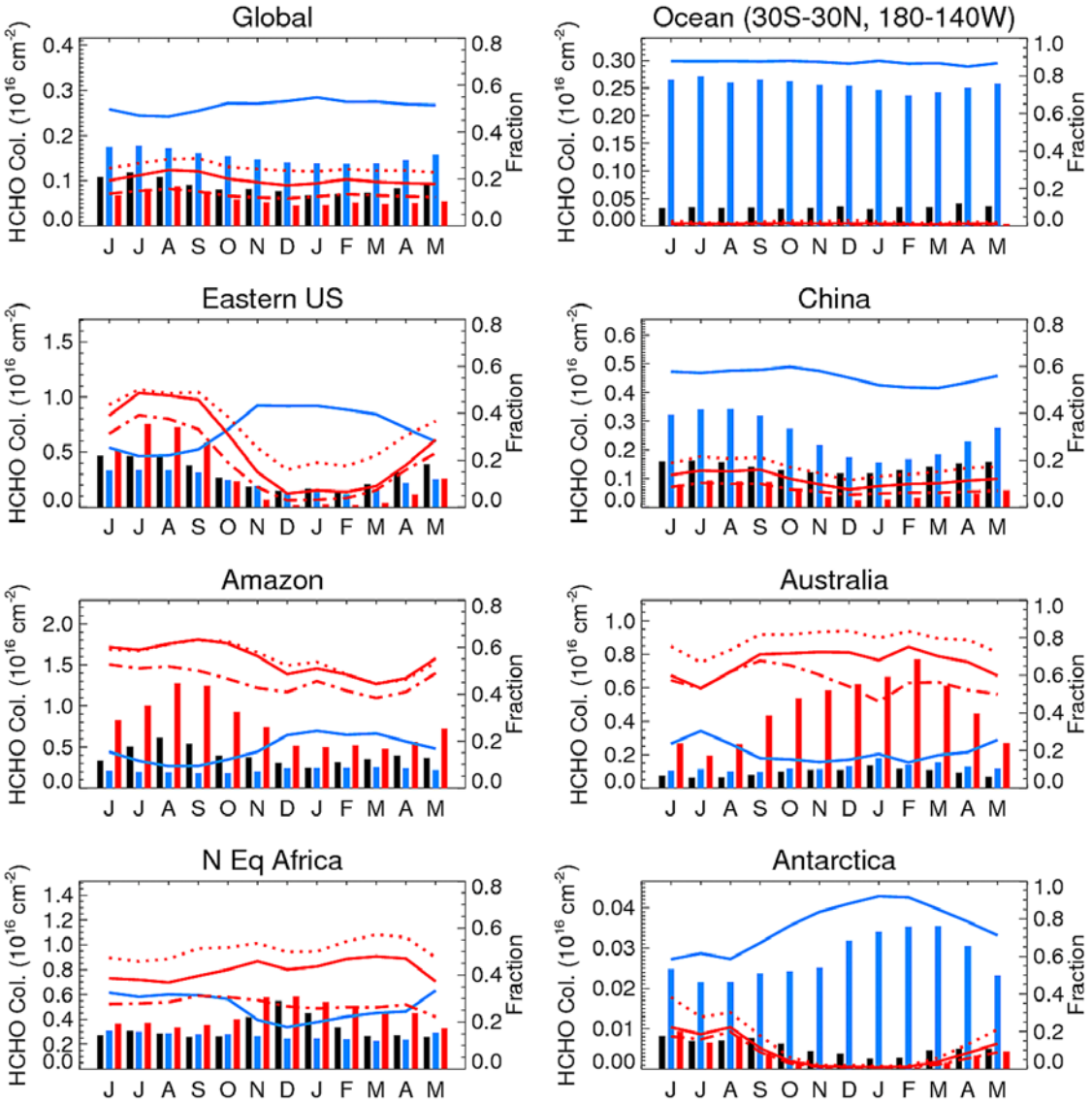

Figure 8. As Figure 5, but for HCHO.

[42] Methane oxidation controls HCHO columns over China and Antarctica. For Antarctica, the HCHO from isoprene sources in Australia and South America is transported toward higher latitudes and contributes to the wintertime peak. Even though absolute amounts of HCHO produced in summertime would be larger, the short lifetime of HCHO during this season prevents long-range transport. This is in contrast to CO, which has a long enough lifetime during summertime to clearly impact the atmospheric composition over Antarctica.

4.3. Nitrogen Species, O_3 and OH

[43] A change in the isoprene emissions will impact the concentrations of OH, thus changing the oxidation capacity of the atmosphere and impacting a large number of atmospheric trace species. The chemical tagging keeps track of species containing carbon from isoprene such as CO or HCHO and also PAN. Regarding other species, e.g., OH, O_3 or NO_x, we are limited to investigating the total concentrations in the three different model simulations because the tagging scheme does not resolve these species.

[44] Without isoprene in the model, the global mean OH concentration below 250 hPa is $9.7 \cdot 10^5$ molecules cm^{-3} and decreases to $9.0 \cdot 10^5$ molecules cm^{-3} when isoprene is included (*MODIS-L*). The average OH concentration for *MODIS-T* is $8.5 \cdot 10^5$ molecules cm^{-3} and $9.4 \cdot 10^5$ molecules cm^{-3} for *CLM*. Most of the decrease in OH when including isoprene is found in the Tropics over the continents, particularly in the boundary layer due to the reaction of OH with isoprene.

[45] PAN is an important reservoir for NO_x and thus has a significant impact on O_3 production. It has no direct sources but is formed in the atmosphere from reactions involving hydrocarbons and nitrogen oxides [*Singh et al.*, 1986]. The global burden (surface to 100 hPa) is estimated as 0.246 Tg N for the *MODIS-L*, as 0.266 Tg N for *MODIS-T* and as 0.22 Tg N for *CLM* (Table 4). The PAN load in the atmosphere is strongly impacted by isoprene, with a contribution of isoprene chemistry to the global annual PAN

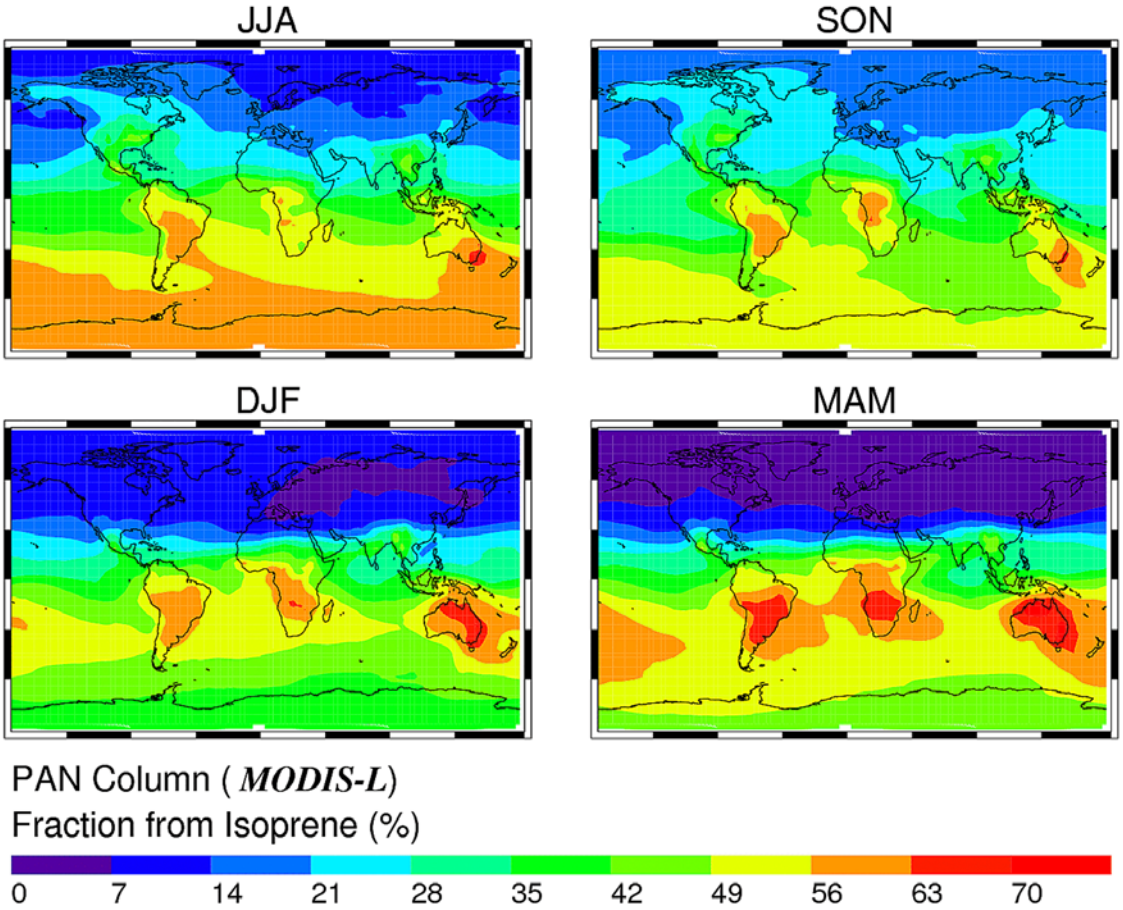

Figure 9. Seasonally varying contribution (%) of isoprene oxidation to the total PAN column (*MODIS-L*).

burden of 29% (32% for *MODIS-T*, 22% for *CLM*) as derived from analysis of the $PAN_{ISOPRENE}$ tracer.

[46] The largest PAN loading is found in the Northern Hemisphere with column amounts of up to 10^{16} molecules cm^{-2} over the industrial areas during spring and summer. Over the Southern Hemisphere, where anthropogenic emissions of NO_x and hydrocarbons are smaller, PAN column amounts range from about $2-5 \cdot 10^{15}$ molecules cm^{-2} with peak values over Equatorial Africa during the biomass burning season comparable to the Northern Hemispheric load. The column contribution of isoprene to PAN (Figure 9) spans a large range and varies from as low as a few percent during Northern Hemispheric winter and spring up to 80% over continental regions in the Southern Hemisphere. During summertime, 20–40% of the PAN over the US is produced from isoprene. Thus simulated PAN can have significant uncertainties associated with uncertainties in the isoprene emissions inventory. For the different isoprene emission scenarios, the PAN column varies by $\sim\pm 2 \cdot 10^{15}$ molecules cm^{-2} or ±40% with largest absolute differences mostly over the industrialized regions of the Northern Hemisphere and biomass burning regions of the Southern Hemisphere.

[47] In Figure 10 we show the time varying contributions of isoprene oxidation to PAN columns for selected regions. The highest impact of isoprene is evident over regions in the Southern Hemisphere with up to 60% of the atmospheric PAN loading explained by isoprene. Nearly half of the PAN loading in the atmosphere over the US in summertime originates from isoprene, but the contribution drops to ~10% in wintertime. Depending on the selection of the LAI and PFT input, the contributions vary by up to 15%.

[48] The formation of PAN from isoprene in the boundary layer or free troposphere above the continents and the subsequent transport are a dominant mechanism for re-distributing NO_x [*Moxim et al.*, 1996]. As a result of NO_x to PAN conversions, the NO_x concentrations over source regions are reduced when adding isoprene, and enhanced over remote areas. The main effect on NO_x is a spatial re-distribution, and globally averaged changes in the NO_x burden between simulations with and without isoprene emissions are small (−0.004 Tg N or <1% of the burden from the surface to 100 hPa). The change in the NO_y (NO_x + NO_3 + HNO_3 + 2 N_2O_5 + HO_2NO_2 + PAN) burden is more pronounced: we estimate an increase of 0.06 Tg N (6% of the burden surface-100 hPa) when isoprene is included mostly due to increased PAN. PAN increases are most pronounced over Equatorial Africa, the Amazon region during fall, and the Eastern US and China during summer and fall.

[49] The global tropospheric burden of O_3 changes only slightly between the three different isoprene emissions scenarios: 398 Tg, 396 Tg and 395 Tg O_3 for *MODIS-L*, *MODIS-T*, and *CLM*, respectively. The burden drops to

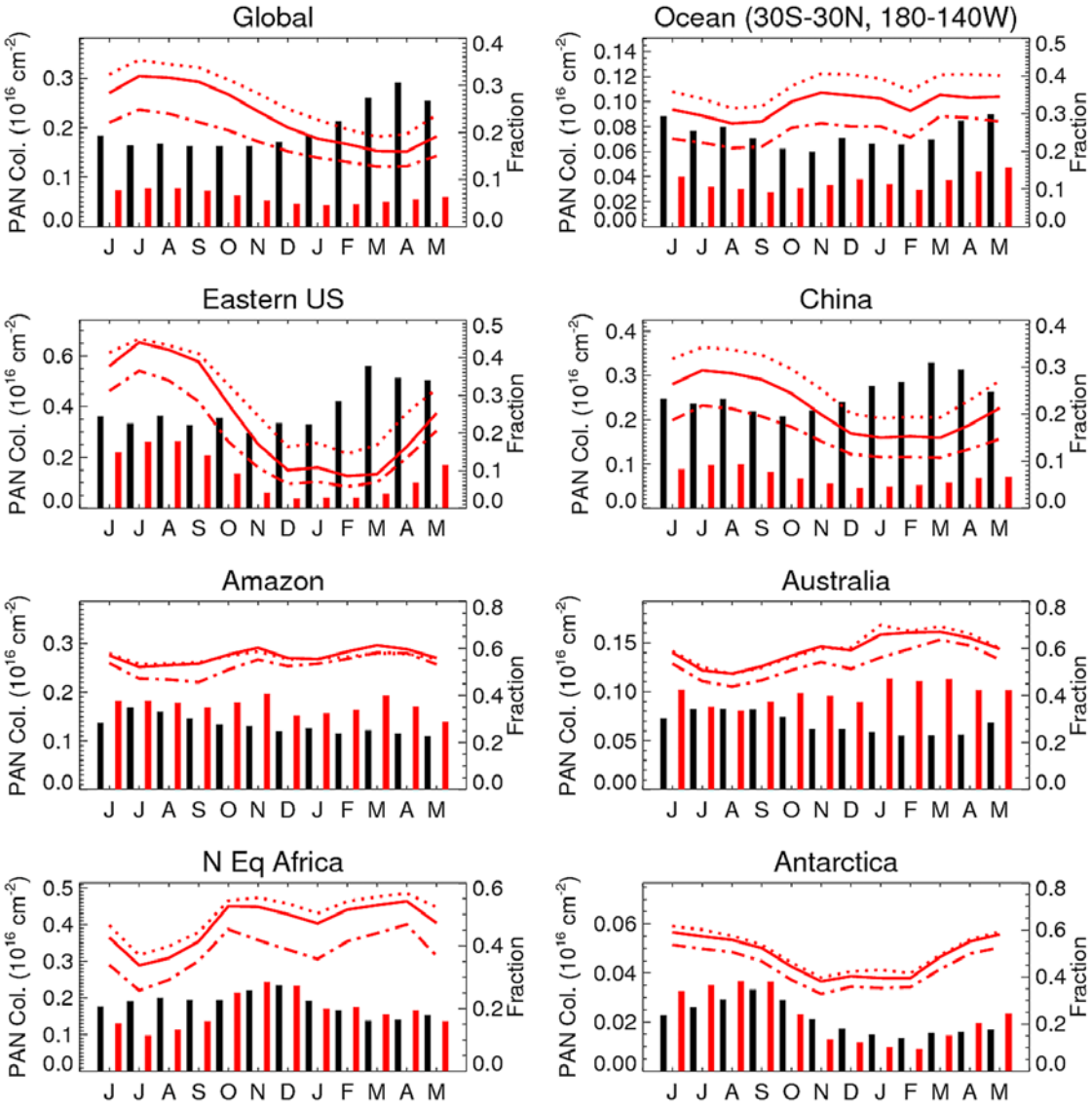

Figure 10. As Figure 5, but for PAN.

385 Tg O_3 for the non-isoprene run, i.e., a reduction by ~3%. The increase in O_3 from isoprene is the result of an increased production rate (492 Tg O_3 a^{-1}) that is in large part compensated for by an increase in the chemical O_3 loss (347 Tg O_3 a^{-1}). The largest relative changes in production and loss are found in the lower troposphere over high isoprene emitting regions. The increased chemical loss with increased isoprene leads to a decrease in the O_3 lifetime. The global average O_3 lifetime for *noISOP* is 32 days and is reduced to 30.5 days for MODIS-L, 30.4 days for MODIS-T and 31 days for CLM.

[50] The results show a small impact on the global budget of O_3, but isoprene can have a significant impact locally. Figure 11 shows the absolute change in the tropospheric O_3 column between the *MODIS-L* simulation and the model run without isoprene. The isoprene-related increase in the tropospheric O_3 column reaches close to 4 DU. The largest changes in O_3 are evident over industrial and biomass burning regions with strong isoprene emissions, where significant biogenic VOC emissions coincide with anthropogenic NO_x emissions [*McKeen et al.*, 1991; *Tao et al.*, 2003] in driving ozone production. Under polluted (high NO_x) conditions the peroxy radicals produced in the oxidation of isoprene convert NO to NO_2 which is then photolyzed to produce O_3.

[51] The largest absolute increase is simulated over Equatorial Africa and the Eastern US (3–4 DU), and the strongest relative increase (10%) is seen over Australia during summertime where some of the highest isoprene emissions are found. It is interesting to note that the model estimates a decrease in O_3 during Southern Hemispheric summer and spring in the Amazon region. South America also has large isoprene emissions but has relatively low NO_x emissions compared to the other high isoprene emitting regions studied. Under these conditions the ozonolysis of isoprene leads to net ozone destruction. This ozone destruction has been observed in other modeling studies as well [*Houweling et al.*, 1998]. Changes related to different isoprene emissions scenarios can be up to ±3 DU, largest uncertainties are evident over Northern Australia.

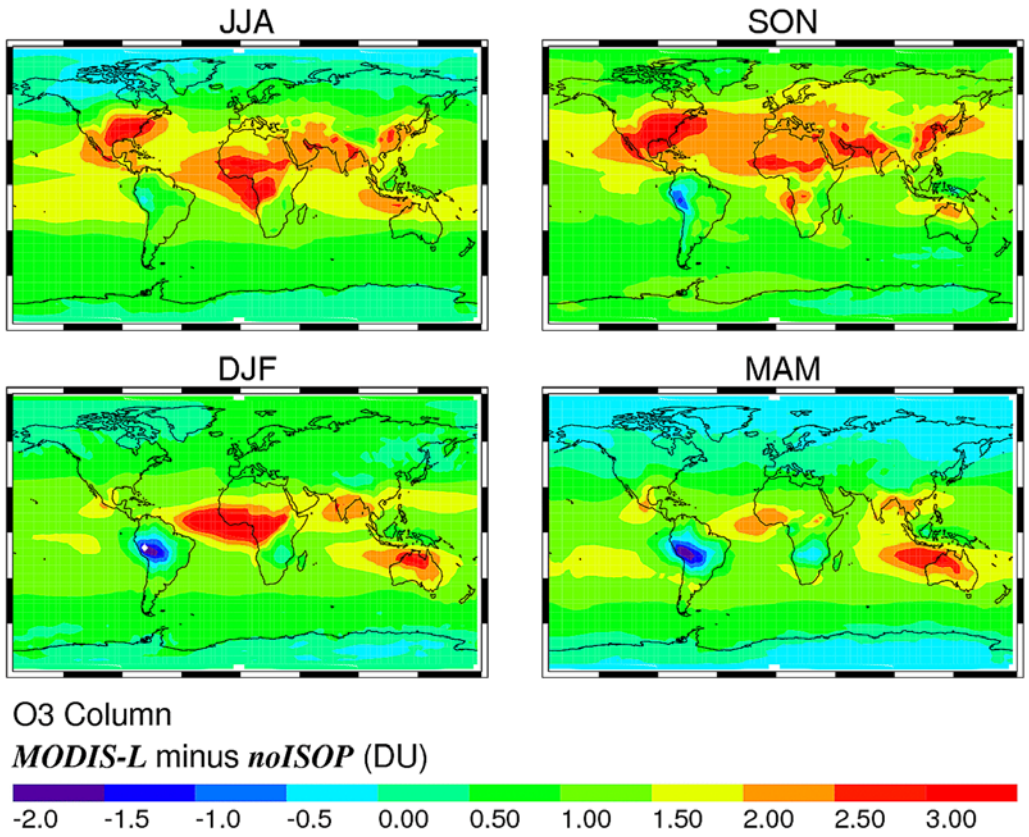

Figure 11. Seasonal difference (DU) in the tropospheric ozone column between model simulations with isoprene (*MODIS-L*) and without isoprene.

[52] Figure 12 shows frequency distributions for differences in the O_3 surface mixing ratio between the various isoprene emission scenarios. When including isoprene, the O_3 surface mixing ratio increases by up to ~10 ppbv and decreases by up to ~5 ppbv over the Amazon region, Indonesia and parts of South Africa during spring. Different LAI and PFT inputs translate into uncertainties of up to ~5 ppbv the surface O_3 concentrations. Comparing the distribution for uncertainties in O_3 to those for CO or HCHO (Figures 4 and 7) the more complex dependence of O_3 on isoprene chemistry is evident. While CO and HCHO are in general directly related to isoprene concentrations, O_3 changes can be either positive or negative.

4.4. Non-Linear Chemistry of CO, HCHO and PAN

[53] Including the tagging scheme allows for the estimation of the actual amount of a chemical species produced from a specified source. As most of the chemical processes in our atmosphere are non-linear, the answer derived from a model tracer is not necessarily identical to the answer derived by subtracting model simulations with and without the considered trace gas source. The simulations we performed provide the necessary information to analyze the extent to which CO, HCHO and PAN are affected by non-linear processes in regard to isoprene emissions.

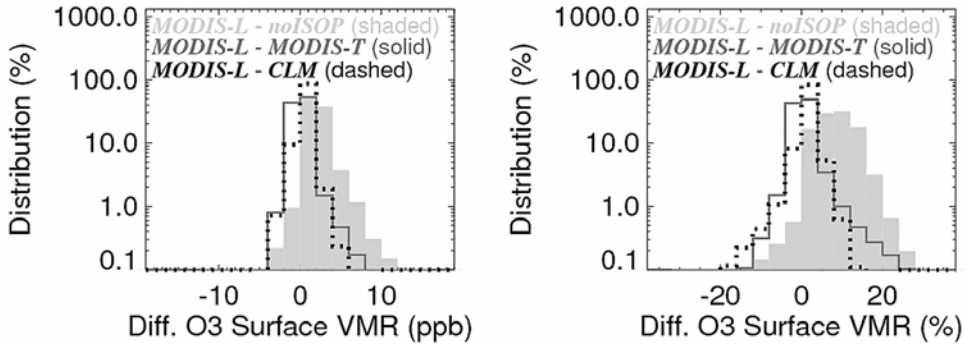

Figure 12. Absolute and relative difference in the O_3 surface mixing ratio between *MODIS-L*, *MODIS-T*, *CLM* and *noISOP* simulations. Distribution functions are calculated from monthly mean O_3 fields.

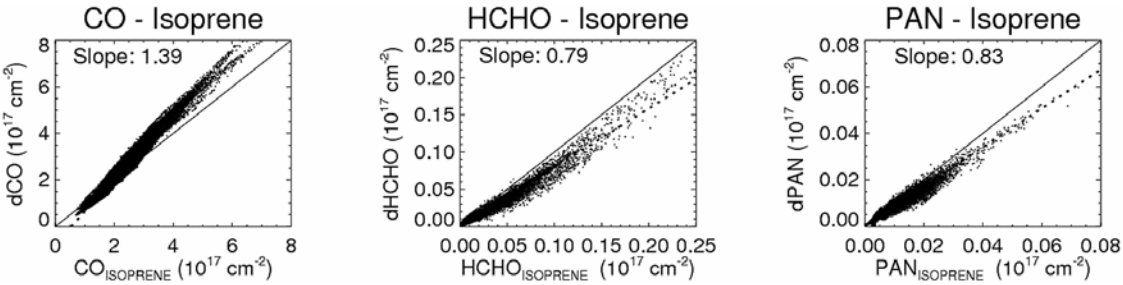

Figure 13. Correlation between the model tracers $CO_{ISOPRENE}$, $HCHO_{ISOPRENE}$ and $PAN_{ISOPRENE}$ and differences in the corresponding species between model simulations with and without isoprene emissions.

[54] Figure 13 shows the relationship between column amounts for the model tracers $CO_{ISOPRENE}$, $HCHO_{ISOPRENE}$, and $PAN_{ISOPRENE}$ and the difference in column amounts dCO, dHCHO, dPAN calculated by subtracting the model run without isoprene emissions from the model run with *MODIS-L* isoprene emissions. Monthly mean values are shown. For all three species we see a slightly non-linear relationship that can be explained for the most part by changes in the atmospheric OH concentrations between model simulations with and without isoprene.

[55] The increase in OH causes a reduced CO load in the model run without isoprene emissions, because of the increased loss of CO and this explains why dCO is larger than $CO_{ISOPRENE}$. The opposite behavior is found for species like HCHO and PAN where direct emissions play a minor or no role and where the production is strongly coupled to atmospheric OH loadings. More OH in the atmosphere increases the production, thus the background levels without isoprene emissions are larger compared to the scenario with isoprene.

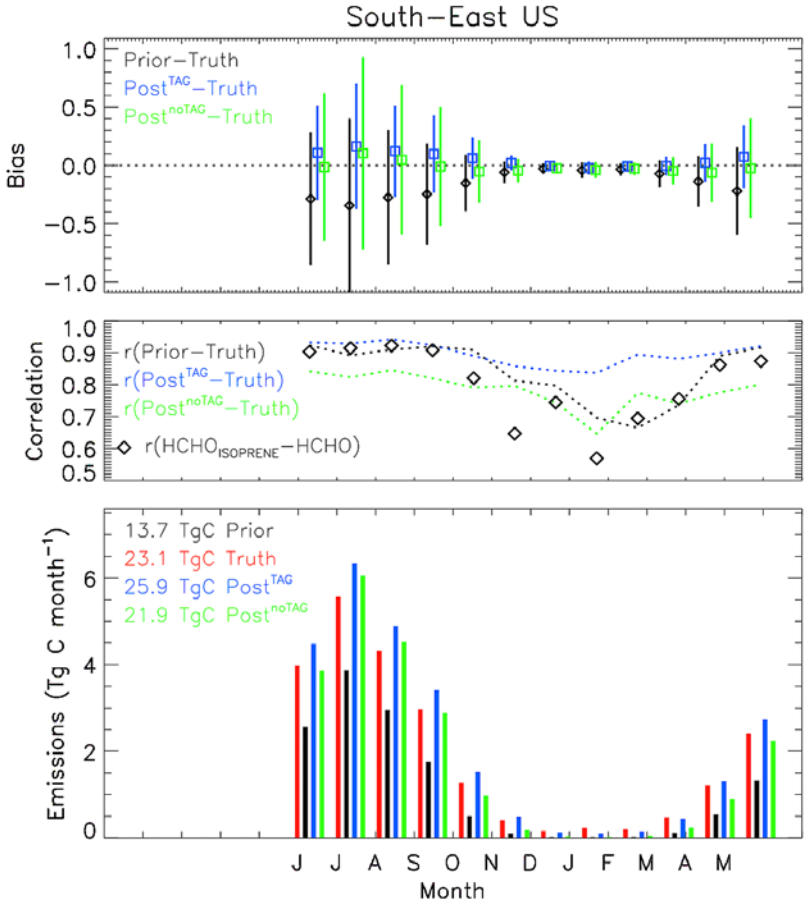

Figure 14. True, priori and posteriori ("Tag" and "noTag" mapping) monthly isoprene emissions over the South-Eastern US (bottom graph). Top graph shows the mean absolute bias and standard deviation between priori and posteriori emissions, middle graph the spatial correlation between the different emissions scenarios as well as the spatial correlation between column amounts of $HCHO_{ISOPRENE}$ and HCHO.

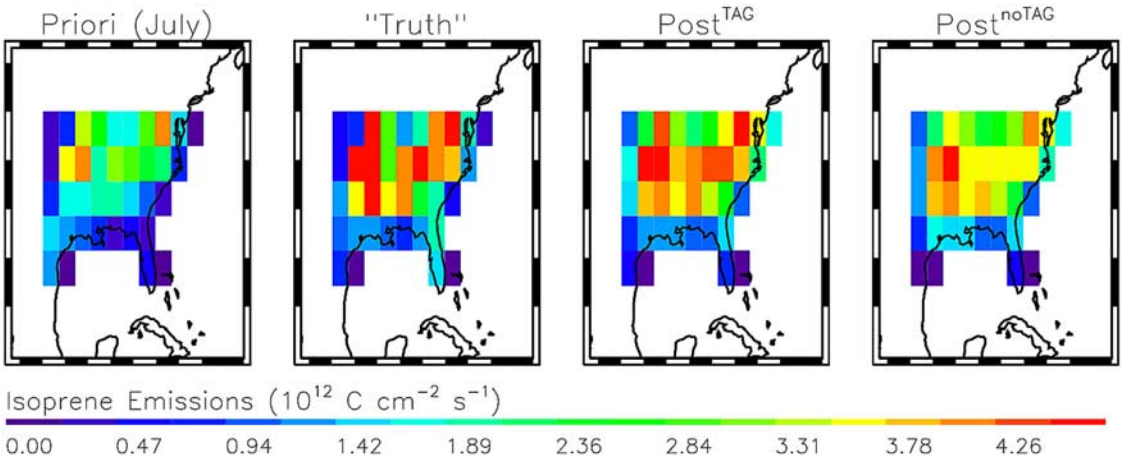

Figure 15. Isoprene emissions over the South-Eastern US in July. From left to right: priori emissions (*CLM*), true emissions (*MODIS-T*), posteriori emissions from "Tag" mapping, posteriori emissions from "noTag" mapping.

[56] The results shown in Figure 13 refer to the total column amount, but discrepancies between tracers and concentration differences vary with location, season and altitude in the atmosphere. For example, the slope calculated from surface volume mixing ratios is 1.18 for CO, 0.78 for HCHO and 0.85 for PAN, and 1.44, 0.58, and 0.77, respectively when using mixing ratios at 500 hPa. The impact of non-linearity on the global average burden is, for the three trace gases considered here, on the order of 10%. The change in the burden (surface-100 hPa) between *MODIS-L* and the simulation without isoprene is 58.5 Tg CO compared to 53.8 Tg $CO_{ISOPRENE}$, i.e., a difference of about 8%. For HCHO we estimate 0.187 Tg HCHO compared to 0.212 Tg $HCHO_{ISOPRENE}$ (−13% difference)

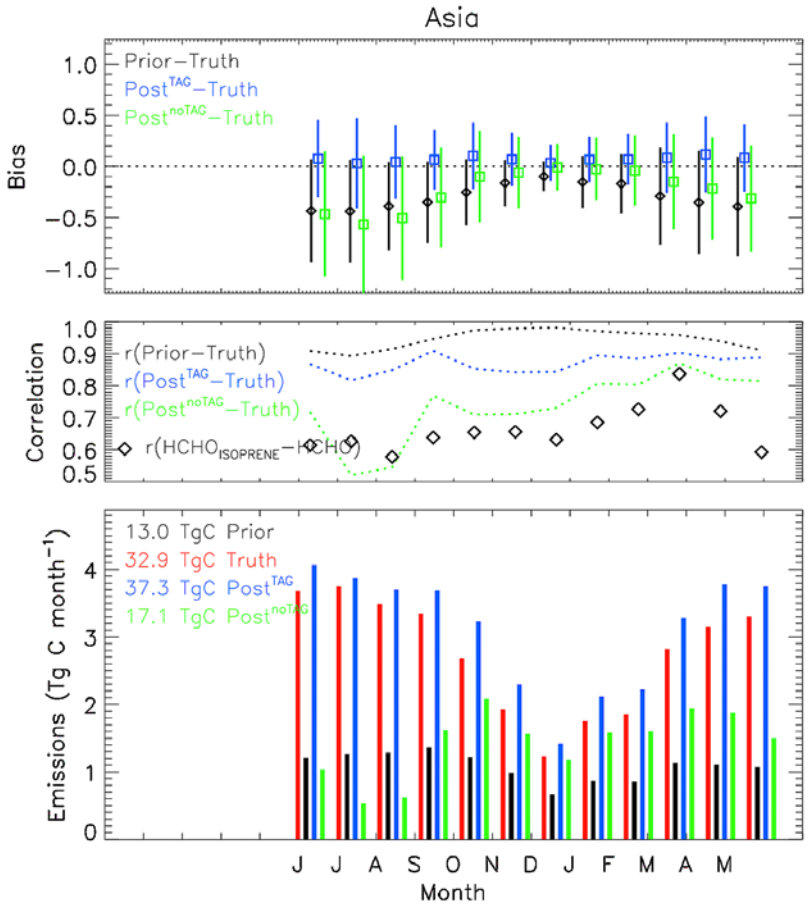

Figure 16. As Figure 14 but for South-East Asia.

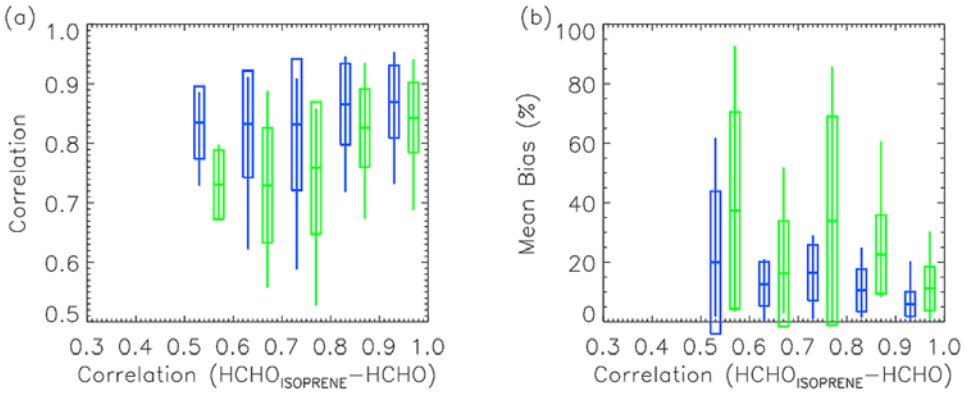

Figure 17. Whisker plots showing: (a) Spatial correlation between posteriori emissions and true emissions as a function of the correlation between the $HCHO_{ISOPRENE}$ and the HCHO column. (b) Mean bias between posteriori emissions and true emissions as a function of the correlation between the $HCHO_{ISOPRENE}$ and the HCHO column. Posteriori "Tag" emissions (blue) and posteriori "noTag" emissions (green).

and for PAN 0.0625 Tg N compared to 0.0703 Tg N of $PAN_{ISOPRENE}$ (−12% difference).

[57] For certain regions the non-linear effect can be more pronounced. In the tropics we find differences between column amounts of $CO_{ISOPRENE}$ and dCO of up to 20–30% ($1.5 \cdot 10^{17}$ molecules cm^{-2}). In areas where $CO_{ISOPRENE}$ is small, i.e., oceanic regions far away from sources or Northern Hemispheric wintertime, we find a slight increase in OH concentrations when including isoprene resulting in slightly larger values for $CO_{ISOPRENE}$ compared to dCO. Regarding the non-linearity in HCHO we find that $HCHO_{ISOPRENE}$ can be lower than dHCHO by up to ∼50% in regions of large HCHO load in the Southern Hemisphere. Thus to avoid large uncertainties in budget analysis non-linear effects need to be taken into account. To what degree information about the non-linearity might improve the constraints of isoprene emissions from HCHO observations is investigated in the following section.

5. Constraining Isoprene Emissions

[58] The results presented in the previous sections show the large uncertainties of current emission estimates for isoprene associated with uncertainties in current assessments of land cover characteristics and their potentially significant influence on atmospheric chemistry, e.g., by affecting concentrations of CO, HCHO, PAN and O_3. Regions with high emissions and high uncertainty include many of the continental areas in the Southern Hemisphere with Australia and equatorial Africa as some of the regions most strongly affected by isoprene, and the summertime Eastern US in the Northern Hemisphere. The findings support a critical need for improved estimates of source magnitude, location, and seasonality of isoprene emissions in order to improve our understanding of the composition of the troposphere. Isoprene has a short lifetime and is difficult to measure on a large scale, and for this reason one has to rely on observations of isoprene oxidation products when constraining its sources on a regional and global scale.

[59] Global and large-scale observations of CO are available with reasonably good quality, but the CO load in the atmosphere is dominated by oxidation of methane and surface emissions. Contributions from isoprene oxidation can be as high as 25% over certain regions (Figure 3). However, with the high variability in surface CO emissions and their large uncertainties, often a factor of 2–3, it is not feasible to use observations of CO to constrain isoprene emissions. PAN columns are strongly impacted by isoprene sources, but large-scale observations of PAN amounts are not available.

[60] Conversely, HCHO column amounts have the potential for fulfilling the given requirements (section 3 and Figure 6). *Palmer et al.* [2003] were the first to employ HCHO column observations of the remote-sensing Global Ozone Monitoring Experiment (GOME) over summertime North America to constrain isoprene emissions. After arguing that (1) the variability in observed HCHO columns is mostly due to isoprene and (2) that the lifetime of HCHO is short enough to assume that HCHO columns are collocated with isoprene sources, they used a chemistry transport model to relate isoprene emissions to HCHO column amounts. The linear relationship between modeled HCHO columns and isoprene emissions is applied as a "transfer function" and then used to derive isoprene emissions from observed HCHO columns.

[61] The chemical tagging scheme developed in this paper has the potential to improve the constraints of isoprene emissions from space-based HCHO observations. Instead of using the relation between total HCHO columns and isoprene emissions in deriving the transfer function we can employ the column amount of $HCHO_{ISOPRENE}$. While previous studies assumed that the variability in total HCHO columns is purely due to variations in isoprene emissions, the tagging scheme specifically relates variations in HCHO columns from isoprene to isoprene emissions and guarantees that the transfer function is not impacted by any other sources. In the following we give a brief demonstration of the applicability of the model tracer scheme to constrain isoprene emissions. A study including actual formaldehyde observations will be the subject of future work.

[62] We perform here a synthetic mapping in which one set of model simulations is used as "observations/truth" and another one as "model". This allows a determination of how well the constraint of isoprene emissions works in a

qualitative way and what improvements can be achieved when including the tagging scheme. We define the HCHO columns calculated using *CLM* as "model" and HCHO columns from *MODIS-T* as "observations". Accordingly, *CLM* isoprene emissions are considered as "a priori" and *MODIS-T* emissions as "truth". Isoprene emissions derived from the transfer function are denoted as "posteriori". We calculate transfer functions from the "model" in two ways: one by relating isoprene emissions to total HCHO columns ("noTag Mapping"), the other by relating isoprene emissions to $HCHO_{ISOPRENE}$ columns ("Tag" Mapping"). Model results for 13:00 local time are used in this study and monthly mean isoprene emissions are derived from mapping of daily values.

[63] Results from this exercise are shown in Figures 14 and 15 for the Southeastern US. Because negative and positive biases over a region could cancel each other when integrated, a qualitative comparison needs to include not only regional emission totals, but also information about spatial correlation and variability. The annual emissions for the Southeastern US case are 13.7 Tg C for the a priori emission scenario and 23.1 Tg C for the true emissions scenario. Both inverted emission inventories give a significant improvement over the a priori: 25.9 Tg C for the "Tag" and 21.9 Tg C for the "noTag" mapping. The part of the HCHO column variability over this region that can be explained by isoprene (Figure 14, middle graph) is about 90% in summertime and this justifies the assumption taken in the "noTag" mapping that most of the variability in HCHO is due to isoprene. As a result, both mapping techniques are close in their estimates. The mean bias is somewhat smaller for the "noTag" posteriori emissions, but the "Tag" posteriori emissions have a smaller standard deviation and higher spatial correlation. The somewhat better representation of spatial patterns in the "Tag" mapping is reflected in Figure 15 showing maps of the different isoprene emission estimates over the Southeastern US in July.

[64] Similar results are achieved over other regions such as South America or Africa where most of the variability in the column amount of HCHO can be explained by isoprene. A slightly different picture is given when factors others than isoprene have a more pronounced impact on the variability in HCHO. As an example we illustrate in Figure 16 mapping results for South-East Asia, where only 60–80% of the variability in HCHO can be explained by isoprene. In this case the "Tag" mapping clearly shows an improvement over the "noTag" mapping in regard to the correlation as well as the magnitude.

[65] In Figure 17 we summarize the results for a set of regions (South-Eastern US, South-East Asia, North and South Equatorial Africa, South America and Australia) by putting the spatial correlation and the mean bias between priori and posteriori emissions and the true emissions in relation to the correlation between $HCHO_{ISOPRENE}$ and HCHO. At high $HCHO_{ISOPRENE}$ -HCHO correlations both sets of posteriori emissions tend to show a high spatial correlation and a small bias. With decreasing $HCHO_{ISOPRENE}$ -HCHO correlation the spatial correlation decreases, due to the imprecise collocation of isoprene sources and HCHO columns, and the bias increases. However, the results show that with decreasing HCHO correlation the "Tag" mapping has generally a higher correlation and a smaller bias compared to the "noTag" mapping indicating that the inclusion of the isoprene tag indeed is a powerful tool to reduce the uncertainties in the constraints of isoprene emissions.

6. Summary

[66] The presented work investigates uncertainties in current emission estimates for isoprene in regard to land classification information and how these uncertainties impact concentrations of key atmospheric species on a large scale. For this purpose the biogenic emissions model MEGAN has been integrated into the chemistry transport model MOZART. We included three different data sets for land classification and land cover characteristics in the emissions model and find that the estimated isoprene emissions range from as low as 310 Tg C a^{-1} to as high as 600 Tg C a^{-1}, depending on the land cover classification. Some of the largest discrepancies are seen over Australia, Africa and the Eastern US. For this analysis, the MOZART model has been extended by a chemical tagging scheme that keeps track of the amount of carbon species produced from isoprene oxidation. This tracer method has the advantage of isolating the sole contribution of isoprene to trace gas budgets.

[67] The results of this modeling exercise show that, depending on the isoprene emission scenario, 9–16% of the global CO burden, 15–27% of the global HCHO burden, and 22–32% of the global PAN burden in the atmosphere is derived from isoprene. Different isoprene emission scenarios translate into uncertainties of up to ±20% in the CO column amount and of ±20% or ±15 ppbv in the surface CO mixing ratio. HCHO has a higher sensitivity to isoprene and we find variability in the column amount on the order of ±50% for different isoprene emission scenarios. For PAN the variations are up to ±40% in the atmospheric column. Regions with the highest uncertainties include Northern Australia and Equatorial Africa. These are regions with high isoprene emissions and large differences in the different vegetation maps. The impacts of isoprene on O_3 are small on a global average; we find that the annual tropospheric burden changes by ~3% due to isoprene and <1% between the different emission scenarios. Regionally, differences can be much more significant. Varying the land classification information in the isoprene emissions model translates into changes of up to 5 ppbv in the O_3 surface mixing ratio and of up to 3 DU in the tropospheric column.

[68] The results of our study point out the potentially high impact of isoprene on the atmospheric composition over certain regions and the need for an improved understanding of the spatial distribution, the magnitude and the seasonality of emissions of isoprene. We find large discrepancies in currently available information about land cover classification, which is an important control of isoprene emission estimates from models and will also impact the estimate of other BVOC emissions. In addition, the model setup we use has the potential for improving constraints of isoprene emissions from observations of HCHO columns as demonstrated by performing a synthetic mapping; Future work will apply this approach to satellite observations of formaldehyde.

[69] **Acknowledgments.** We acknowledge Yuhong Tian for providing input data and Brian Ridley and Christine Wiedinmyer for valuable input to the manuscript. We also like to thank the reviewers for their constructive comments. This material is based upon work supported by the National Aeronautics and Space Administration under Contract No. NNG04GO58G issued through the Earth Observing System Program. NCAR is operated by the University Corporation for Atmospheric Research under sponsorship of the National Science Foundation.

References

Abbot, D. S., P. I. Palmer, R. V. Martin, K. V. Chance, D. J. Jacob, and A. Guenther (2003), Seasonal and interannnual variability of North American isoprene emissions as determined by formaldehyde column measurements from space, *Geophys. Res. Lett.*, *30*(17), 1886, doi:10.1029/2003GL017336.

Atkinson, R. (1997), Gas-phase tropospheric chemistry of volatile organic compounds: 1. Alkanes and Alkenes, *J. Phys. Chem. Ref. Data*, *26*, 215–290.

Atkinson, R., and J. Arey (1998), Atmospheric chemistry of biogenic organic compounds, *Acc. Chem. Res.*, *31*, 574–583.

Bergamaschi, P., R. Hein, M. Heimann, and P. J. Crutzen (2000), Inverse modeling of the global CO cycle 1. Inversion of CO mixing ratios, *J. Geophys. Res.*, *105*, 1909–1927.

Bonan, G. B., K. W. Oleson, M. Vertenstein, S. Levis, X. Zeng, Y. Dai, R. E. Dickinson, and Z. L. Yang (2002a), The land surface climatology of the community land model coupled to the NCAR community climate model, *J. Clim.*, *15*, 3123–3149.

Bonan, G. B., S. Levis, L. Kergoat, and K. W. Oleson (2002b), Landscapes as patches of plant functional types: An integrated concept for climate and ecosystem models, *Global Biogeochem. Cycles*, *16*(2), 1021–1051, 1021, doi:10.1029/2000GB001360.

Cantrell, C., R. Shetter, and J. Calvert (1993), Peroxy radicals as measured in ROSE and estimated from photostationary state deviations, *J. Geophys. Res.*, *98*, 18,355–18,366.

Chance, K., P. I. Palmer, R. J. D. Spurr, R. V. Martin, T. P. Kurosu, and D. J. Jacob (2000), Satellite observations of formaldehyde over North America from GOME, *Geophys. Res. Lett.*, *27*, 3461–3464.

Chen, X., D. Hulbert, and P. B. Shepson (1998), Measurement of the organic nitrate yield from OH reaction with isoprene, *J. Geophys. Res.*, *103*(D19), 25,563–25,568.

Chuong, B., and P. S. Stevens (2002), Measurements of the kinetics of the OH-initiated oxidation of isoprene, *J. Geophys. Res.*, *107*(D13), 4162, doi:10.1029/2001JD000865.

Constable, J. V. H., A. B. Guenther, D. S. Schimel, and R. K. Monson (1999), Modelling changes in VOC emission in response to climate change in the continental United States, *Global Change Biol.*, *5*(7), 791–806, doi:10.1046/j.1365-2486.1999.00273.

Dlugokencky, E. J., R. C. Myers, P. M. Lang, K. A. Masarie, A. M. Crotwell, K. W. Thoning, B. D. Hall, J. W. Elkins, and L. P. Steele (2005), Conversion of NOAA atmospheric dry air methane mole fractions to a gravimetrically-prepared standard scale, *J. Geophys. Res.*, *110*, D18306, doi:10.1029/2005JD006035.

Dlugokencky, E. J., P. M. Lang, and K. A. Masarie (2007), Atmospheric Methane Dry Air Mole Fractions from the NOAA ESRL Carbon Cycle Cooperative Global Air Sampling Network, 1983–2006, Version: 2007-07-31. Path: ftp://ftp.cmdl.noaa.gov/ccg/ch4/flask/event/

Duncan, B. N., J. A. Logan, I. Bey, I. A. Megretskaia, R. M. Yantosca, P. C. Novelli, N. B. Jones, and C. P. Rinsland (2007), The global budget of CO, 1988–1997: source estimates and validation with a global model, *J. Geophys. Res.*, *112*, D22301, doi:10.1029/2007JD008459.

Edwards, D. P., et al. (2004), Observations of carbon monoxide and aerosols from the Terra satellite: Northern Hemisphere variability, *J. Geophys. Res.*, *109*, D24202, doi:10.1029/2004JD004727.

Edwards, D. P., G. Pétron, P. C. Novelli, L. K. Emmons, J. C. Gille, and J. R. Drummond (2006), Southern Hemisphere carbon monoxide interannual variability observed by Terra/Measurement of Pollution in the Troposphere (MOPITT), *J. Geophys. Res.*, *111*, D16303, doi:10.1029/2006JD007079.

Fan, J., and R. Zhang (2004), Atmospheric oxidation mechanism of isoprene, *Environ. Chem.*, *1*(3), 140–149.

Fehsenfeld, F., et al. (1992), Emissions of volatile organic compounds from vegetation and the implications for atmospheric chemistry, *Global Biogeochem. Cycles*, *6*(4), 389–430, doi:10.1029/92GB02125.

Fiore, A. M., L. W. Horowitz, D. W. Purves, H. Levy II, M. J. Evans, Y. Wang, Q. Li, and R. M. Yantosca (2005), Evaluating the contribution of changes in isoprene emissions to surface ozone trends over the eastern United States, *J. Geophys. Res.*, *110*, D12303, doi:10.1029/2004JD005485.

Folberth, G. A., D. A. Hauglustaine, J. Lathiere, and F. Brochetone (2005), Impact of biogenic hydrocarbons on tropospheric chemistry: Results from a global chemistry-climate model, *Atmos. Chem. Phys. Discuss.*, *5*, 10,517–10,612.

Giorgi, F., and W. L. Chameides (1985), The rainout parameterization in a photochemical model, *J. Geophys. Res.*, *90*, 7872–7880.

Granier, C., G. Petron, J.-F. Müller, and G. Brasseur (2000), The impact of natural and anthropogenic hydrocarbons on the tropospheric budget of carbon monoxide, *Atmos. Environ.*, *34*, 5255–5270.

Granier, C., et al. (2004), Present and future surface emissions of atmospheric compounds, European Commission report EVK 2199900011. (Available at http://www.aero.jussieu.fr/projet/ACCENT/POET.php)

Griffin, R. J., III, J. H. Seinfeld, and D. Dabdub (1999), Estimate of global atmospheric organic aerosol from oxidation of biogenic hydrocarbons, *Geophys. Res. Lett.*, *26*(17), 2721–2724, doi:10.1029/1999GL900476.

Guenther, A., T. Karl, P. Harley, C. Wiedinmyer, P. I. Palmer, and C. Geron (2006), Estimates of global terrestrial isoprene emissions using MEGAN (Model of Emissions of Gases and Aerosols from Nature), *Atmos. Chem. Phys.*, *6*, 3181–3210.

Guenther, A. B., P. R. Zimmermann, P. C. Harley, R. K. Monsoon, and R. Fall (1993), Isoprene and monoterpene emission rate variability - Model evaluations and sensitivity analyses, *J. Geophys. Res.*, *98*(D7), 12,609–12,617.

Guenther, A., et al. (1995), A global model of natural volatile organic compound emissions, *J. Geophys. Res.*, *100*(D5), 8873–8892, doi:10.1029/94JD02950.

Harley, P. C., M. E. Litvak, T. D. Sharkey, and R. K. Monson (1994), Isoprene emissions from velvet bean-leaves - Interactions among nitrogen availability, growth photon flux density and leaf development, *Plant Physiol.*, *105*(1), 279–285.

Henze, D. K., and J. H. Seinfeld (2006), Global secondary organic aerosol from isoprene oxidation, *Geophys. Res. Lett.*, *33*, L09812, doi:10.1029/2006GL025976.

Hoffmann, T., R. Bandur, U. Marggraf, and M. Linscheid (1998), Molecular composition of organic aerosols formed in the alpha-pinene/ O_3 reaction: Implications for new particle formation processes, *J. Geophys. Res.*, *103*(D19), 25,569–25,578, doi:10.1029/98JD01816.

Horowitz, L. W., J. Liang, G. M. Gardner, and D. J. Jacob (1998), Export of reactive nitrogen from North America during summertime: Sensitivity to hydrocarbon chemistry, *J. Geophys. Res.*, *103*, 13,451–13,376.

Horowitz, L. W., A. M. Fiore, G. P. Milly, R. C. Cohen, A. Perring, P. J. Wooldridge, P. G. Hess, L. K. Emmons, and J.-F. Lamarque (2007), Observational constraints on the chemistry of isoprene nitrates over the eastern United States, *J. Geophys. Res.*, *112*, D12S08, doi:10.1029/2006JD007747.

Horowitz, L., et al. (2003), A global simulation of tropospheric ozone and related tracers: Description and evaluation of MOZART, version 2, *J. Geophys. Res.*, *108*(D24), 4784, doi:10.1029/2002JD002853.

Houweling, S., F. Dentener, and J. Lelieveld (1998), The impact of nonmethane hydrocarbon compounds on tropospheric photochemistry, *J. Geophys. Res.*, *103*(D9), 10,673–10,696, doi:10.1029/97JD03582.

Ito, A., S. Sillman, and J. E. Penner (2007), Effects of additional nonmethane volatile organic compounds, organic nitrates, and direct emissions of oxygenated organic species on global tropospheric chemistry, *J. Geophys. Res.*, *112*, D03609, doi:10.1029/2005JD006556.

Justice, C. O., J. R. G. Townshend, E. F. Vermote, E. Masuoka, R. E. Wolfe, N. Saleous, D. P. Roy, and J. T. Morisette (2002), An overview of MODIS land processing and product status, *Remote Sens. Environ.*, *83*, 3–15.

Kanamitsu, M. (1989), Description of the NMC global data assimilation and forecast system, *Weather and Forecasting*, *4*, 335–342.

Kroll, J. H., N. L. Ng, S. M. Murphy, R. C. Flagan, and J. H. Seinfeld (2005), Secondary organic aerosol formation from isoprene photooxidation under high NOx conditions, *Geophys. Res. Lett.*, *32*, L18808, doi:10.1029/2005GL023637.

Kroll, J. H., N. L. Ng, S. M. Murphy, R. C. Flagan, and J. H. Seinfeld (2006), Secondary organic aerosol formation from isoprene photooxidation, *Environ. Sci. Technol.*, *40*, 1869–1877, doi:10.1021/es0524301.

Lawrence, P. J., and T. N. Chase (2007), Representing a new MODIS consistent land surface in the Community Land Model (CLM 3.0), *J. Geophys. Res.*, *112*, G01023, doi:10.1029/2006JG000168.

Lerdau, M., A. Guenther, and R. Monson (1997), Production and emission of volatile organic compounds by plants, *Bioscience*, *47*, 373–383.

Levis, S., C. Wiedinmyer, G. B. Bonan, and A. Guenther (2003), Simulating biogenic volatile organic compound emissions in the Community Climate System Model, *J. Geophys. Res.*, *108*(D21), 4659, doi:10.1029/2002JD003203.

Liang, J., L. W. Horowitz, D. J. Jacob, Y. Wang, A. M. Fiore, J. A. Logan, G. M. Gardner, and J. W. Munger (1998), Seasonal variations of reactive nitrogen species and ozone over the Unites States, and export fluxes to the global atmosphere, *J. Geophys. Res.*, *103*, 13,435–13,450.

McKeen, S. A., E.-Y. Hsie, and S. C. Liu (1991), A study of the dependence of rural ozone on ozone precursors in the eastern United States, *J. Geophys. Res.*, *96*, 15,377–15,394.

Miyoshi, A., S. Hatakeyama, and N. Washida (1994), OH radical-initiated photooxidation of isoprene: An estimate of global CO production, *J. Geophys. Res.*, *99*(D9), 18,779–18,788, doi:10.1029/94JD01134.

Monson, R., P. Harley, M. Litvak, M. Wildermuth, A. Guenther, P. Zimmermann, and R. Fall (1994), Environmental and developmental controls over the seasonal pattern of isoprene emission from aspen leaves, *Oecologica*, *99*, 260–270.

Moxim, W., H. Levy II, and P. S. Kasibhatla (1996), Simulated global tropospheric PAN: Its transport and impact on NO_x, *J. Geophys. Res.*, *101*(D7), 12,621–12,638, doi:10.1029/96JD00338.

Oleson, K. W., G. B. Bonan, C. Schaaf, F. Gao, Y. Jin, and A. Strahler (2003), Assessment of global climate model land surface albedo using MODIS data, *Geophys. Res. Lett.*, *30*(8), 1443, doi:10.1029/2002GL016749.

Orlando, J. J., G. S. Tyndall, and T. J. Wallington (2003), The atmospheric chemistry of alkoxy radicals, *Chem. Rev.*, *103*, 4657–4690.

Palmer, P. I., D. J. Jacob, A. M. Fiore, R. V. Martin, K. Chance, and T. P. Kurosu (2003), Mapping isoprene emissions over North America using formaldehyde column observations from space, *J. Geophys. Res.*, *108*(D6), 4180, doi:10.1029/2002JD002153.

Patchen, A. K., M. J. Pennino, A. C. Kiep, and M. J. Elrod (2007), Direct kinetics study of the product-forming channels of the reaction of isoprene-derived hydroxyperoxy radicals with NO, *Int. J. Chem. Kin.*, *39*, 353–361.

Pétron, G., P. Harley, J. Greenberg, and A. Guenther (2001), Seasonal temperature variations influence isoprene emission, *Geophys. Res. Lett.*, *28*(9), 1707–1710.

Pétron, G., C. Granier, B. Khattotov, V. Yudin, J.-F. Lamarque, L. Emmons, J. Gille, and D. P. Edwards (2004), Monthly CO surface sources inventory based on the 2000–2001 MOPITT satellite data, *Geophys. Res. Lett.*, *31*, L21107, doi:10.1029/2004GL020560.

Pfister, G., P. G. Hess, L. K. Emmons, J.-F. Lamarque, C. Wiedinmyer, D. P. Edwards, G. Petron, J. C. Gille, and G. W. Sachse (2005), Constraints on emissions for the Alaskan wildfires 2004 using data assimilation and inverse modeling of MOPITT CO, *Geophys. Res. Lett.*, *32*(11), L11809, doi:10.1029/2005GL022995.

Pfister, G. G., et al. (2006), Ozone production from the 2004 North American boreal fires, *J. Geophys. Res.*, *111*, D24S07, doi:10.1029/2006JD007695.

Pierce, T., C. Geron, L. Bender, R. Dennis, G. Tonnesen, and A. Guenther (1998), Influence of increased isoprene emissions on regional ozone modeling, *J. Geophys. Res.*, *103*, 25,611–25,629.

Potter, C. S., S. E. Alexander, J. C. Coughlan, and S. A. Klooster (2001), Modeling biogenic isoprene: Exploration of model drivers, climate control algorithms, and use of global satellite observations, *Atmos. Environ.*, *35*, 6151–6165.

Rosenstiel, T. N., M. J. Potosnak, K. L. Griffin, R. Fall, and R. K. Monson (2003), Increased CO2 uncouples growth from isoprene emission in an agriforest ecosystem, *Nature*, *421*, 256–259.

Sanderson, M. G., W. J. Collins, R. G. Derwent, and C. E. Johnson (2003), Simulation of global hydrogen levels using a Lagrangian three-dimensional model, *J. Atmos. Chem.*, *46*, 15–28.

Sharkey, T. D., E. L. Singsaas, M. T. Lerdau, and C. Geron (2000), Weather effects on isoprene emission capacity and applications in emissions algorithms, *Ecol. Appl.*, *9*, 1132–1137.

Shim, C., Y. Wang, Y. Choi, P. I. Palmer, D. S. Abbot, and K. Chance (2005), Constraining global isoprene emissions with Global Ozone Monitoring Experiment (GOME) formaldehyde column measurements, *J. Geophys. Res.*, *110*, D24301, doi:10.1029/2004JD005629.

Singh, H. B., L. J. Salas, and W. Viezee (1986), Global distribution of peroxyacetyl nitrate, *Nature*, *321*, 588–591.

Sparks, J. P., J. M. Roberts, and R. K. Monson (2003), The uptake of gaseous organic nitrogen by leaves: A significant global nitrogen transfer process, *Geophys. Res. Lett.*, *30*(23), 2189, doi:10.1029/2003GL018578.

Sprengnether, M., K. L. Demerjian, N. M. Donahue, and J. G. Anderson (2002), Product analysis of the OH oxidation of isoprene and 1,3-butadiene in the presence of NO, *J. Geophys. Res.*, *107*(D15), 4268, doi:10.1029/2001JD000716.

Tao, Z., S. M. Larson, D. J. Wuebbles, A. Williams, and M. Caughey (2003), A summer simulation of biogenic contributions to ground-level ozone over the continental United States, *J. Geophys. Res.*, *108*(D14), 4404, doi:10.1029/2002JD002945.

Tian, Y., R. E. Dickinson, L. Zhou, R. B. Myneni, M. Friedl, C. B. Schaaf, M. Carroll, and F. Gao (2004), Land boundary conditions from MODIS data and consequences for the albedo of a climate model, *Geophys. Res. Lett.*, *31*(5), L05504, doi:10.1029/2003GL019104.

Tuazon, E. C., and R. Atkinson (1996), A product study of the gas-phase reaction of isoprene with the OH radical in the presence of NO_x, *Int. J. Chem. Kinet.*, *22*, 1221–1236.

van der Werf, G. R., J. T. Randerson, L. Giglio, G. J. Collatz, P. S. Kasibhatla, and A. F. Arellano Jr. (2006), Interannual variability of global biomass burning emissions from 1997 to 2004, *Atmos. Chem. Phys.*, *6*, 3423–3441.

Velikova, V., P. Pinelli, S. Pasqualini, L. Reale, and F. Ferranti (2005), Isoprene decreases the concentration of nitric oxide in leaves exposed to elevated ozone, *New Phytologist*, *166*(2), 419–426.

von Kuhlmann, R., M. G. Lawrence, U. Pöschl, and P. J. Crutzen (2004), Sensitivities in global scale modeling of isoprene, *Atmos. Chem. Phys.*, *4*, 1–17.

Walmsley, J. L., and M. L. Wesely (1996), Modification of coded parameterizations of surface resistances to gaseous dry deposition, *Atmos. Environ.*, *30*, 1181–1188.

Warneck, P. (2000), *Chemistry of the Natural Atmosphere*, 927 pp, Academic, San Diego, California.

Wesely, M. L. (1989), Parameterization of surface resistances to gaseous dry deposition in regional-scale numerical models, *Atmos. Environ.*, *23*, 1293–1304.

Wesely, M. L., and B. B. Hicks (2000), A review of the current status of knowledge on dry deposition, *Atmos. Environ.*, *34*, 2261–2282.

Wu, S., L. J. Mickley, D. J. Jacob, J. A. Logan, R. M. Yantosca, and D. Rind (2007), Why are there large differences between models in global budgets of tropospheric ozone?, *J. Geophys. Res.*, *112*, D05302, doi:10.1029/2006JD007801.

L. K. Emmons, A. Guenther, P. G. Hess, J.-F. Lamarque, J. J. Orlando, G. G. Pfister, and S. Walters, National Center for Atmospheric Research, Boulder, CO 80307-3000, USA. (pfister@ucar.edu)

P. J. Lawrence, Cooperative Institute for Research in Environmental Sciences (CIRES), University of Colorado, Boulder, CO, USA.

P. I. Palmer, School of GeoSciences, University of Edinburgh, Edinburgh, UK.